Journal of *Marine Science and Engineering*

MDPI

Article

Unleashing the Potential of a Hybrid 3D Hydrodynamic Monte Carlo Risk Model for Maritime Structures' Design in the Imminent Climate Change Era

Arif Uğurlu [1,*], Egemen Ander Balas [2], Can Elmar Balas [3] and Sami Oğuzhan Akbaş [3]

[1] General Directorate of Infrastructure Investments, Ministry of Transport and Infrastructure, 06490 Ankara, Türkiye
[2] Faculty of Engineering, Department of Civil Engineering, Başkent University, 06790 Ankara, Türkiye; eanderbalas@baskent.edu.tr
[3] Sea and Aquatic Sciences Application and Research Center, Gazi University, 06570 Ankara, Türkiye; cbalas@gazi.edu.tr (C.E.B.); soakbas@gazi.edu.tr (S.O.A.)
* Correspondence: arif.ugurlu@uab.gov.tr

Abstract: Submarine pipelines have become integral for transporting resources and drinking water across large bodies. Therefore, ensuring the stability and reliability of these submarine pipelines is crucial. Incorporating climate change impacts into the design of marine structures is paramount to assure their lifetime safety and serviceability. Deterministic design methods may not fully consider the uncertainties and risks related to climate change compared to risk-based design models. The latter approach considers the future risks and uncertainties linked to climate and environmental changes, thus ensuring infrastructure sustainability. This study pioneers a Hybrid 3D Hydrodynamic Monte Carlo Simulation (HMCS) Model to improve the reliability-based design of submarine pipelines, incorporating the effects of climate change. Current design approaches may follow deterministic methods, which may not systematically account for climate change's comprehensive uncertainties and risks. Similarly, traditional design codes often follow a deterministic approach, lacking in the comprehensive integration of dynamic environmental factors such as wind, waves, currents, and geotechnical conditions, and may not adequately handle the uncertainties, including the long-term effects of climate change. Nowadays, most countries are developing new design codes to modify the risk levels for climate change's effects, such as sea-level rises, changes in precipitation, or changes in the frequency/intensity of winds/storms/waves in coastal and marine designs. Our model may help these efforts by integrating a comprehensive risk-based approach, utilizing a 3D hydrodynamic model to correlate diverse environmental factors through Monte Carlo Simulations (MCS). The hybrid model can promise the sustainability of marine infrastructure by adapting to future environmental changes and uncertainties. Including such advanced methodologies in the design, codes are encouraged to reinforce the resilience of maritime structures in the climate change era. The present design codes should inevitably be reviewed according to climate change effects, and the hybrid risk-based design model proposed in this research should be included in codes to ensure the reliability of maritime structures. The HMCS model represents a significant advancement over existing risk models by incorporating comprehensive environmental factors, utilizing advanced simulation techniques, and explicitly addressing the impacts of climate change. This innovative approach ensures the development of more resilient and sustainable maritime infrastructure capable of withstanding future environmental uncertainties.

Keywords: climate change impacts; wave climate variability; disruptive effects of lake level changes; future changes in wave climate; Hydrotam-3D

check for updates

Citation: Uğurlu, A.; Balas, E.A.; Balas, C.E.; Akbaş, S.O. Unleashing the Potential of a Hybrid 3D Hydrodynamic Monte Carlo Risk Model for Maritime Structures' Design in the Imminent Climate Change Era. *J. Mar. Sci. Eng.* **2024**, *12*, 931. https://doi.org/10.3390/jmse12060931

Academic Editors: Dong-Sheng Jeng and Dong-Jiing Doong

Received: 18 April 2024
Revised: 24 May 2024
Accepted: 27 May 2024
Published: 31 May 2024

1. Introduction

The infrastructure across large water bodies, either for the movement of resources or drinkable water, is significantly dependent upon submarine pipelines. But, at the same time, it brings a variety of environmental risks to which they are exposed, including climate change. Therefore, these structures may be designed with a risk approach that would include the impact of climate change and environmental uncertainties by giving the designer the future impacts on the structure. A risk-based approach will enable the engineer to design a submarine pipeline that will be more resilient to the prevailing effects of climate change. The HMCS model is a hybrid methodology that can be used for the risk-based design.

The model can consider environmental factors that have a key influence on the stability of the submarine pipeline by using the sub-models that comprise wind, waves, current, geotechnical conditions, and climate changes. Hydrotam-3D is a three-dimensional model that can be employed to assess the environmental conditions of maritime structures and the effects of climate change to design them to be resilient in the climate change era.

Reliability-based assessment methodologies have gained attention in the evaluation of pipeline stability. Ref. [1] evaluated the on-bottom pipeline stability using the MCS for the limit state equations. They also looked upon some other studies regarding the instability of the pipelines, considering the forces of waves, the soil–pipe interaction, and changes in the climate as the variable factors. The research conducted by [2] includes numerical modeling to investigate the behavior of pipeline stability under different soil conditions that play a predominant role in design. Ref. [2] investigated the wave forces acting on submarine pipelines by simulating the wave and structure interaction under various conditions.

A probabilistic model for submarine pipelines was developed by [3] to integrate environmental uncertainties by adopting an MCS-based approach. Ref. [4] developed a method for assessing the reliability of submarine pipelines considering ice loads. Ref. [5] considered the uplift resistance of the pipelines trenched in cohesionless soil, in which the MCS obtained the random variables for the probabilistic solution. Ref. [6] presented a probabilistic analysis of the Turk Stream pipeline system beneath the seabed and compared their exact solution with a probabilistic one.

Ref. [7] computed the uncertainties for safety factors used in a pipeline design against explosions due to the material's strength. They intended to investigate the probability of the pipe explosion using an MCS. Ref. [8] presented a probabilistic method for submarine pipeline stability. The MCS was used to solve the limit state equations and evaluate the pipeline stability, which was implemented at the bottom. Ref. [9] stated that lake warming rates reflect global climatological trends, including the recent warming hiatus. Ref. [10] emphasized that climate change and global warming significantly affected the decrease of Mean Lake Levels (MLL). Ref. [11] discussed the impacts of climate change on coastal and offshore petroleum infrastructures.

Hence, the uncertainties inherent in the design of underwater pipelines are challenging when climate change is considered. The design is affected by soil parameters, wave and current forces, lake area loss due to global warming, and pipeline characteristics. In the scope of this study, the Burdur Lake Water Pipeline Project has been investigated as a case study for the new hybrid model. The project will provide drinking water to the greater province of Burdur. The previous pipeline constructed on the same site lost its function because the decreased water levels due to global warming caused the pipeline to be exposed to breaking waves, and the effect of breaking waves combined with increasing storm intensity caused the pipeline rupture, as shown in Figure 1.

Although the originally designed pipeline was located on the lakebed, the proposed replacement is located on the shore area due to water withdrawal related to global warming. However, because the region is a lakebed, there is a possibility that it will be underwater again in the future.

Thus, the Burdur Lake pipeline design was conducted using the new hybrid design model, which incorporates the uncertainties associated with climate change for the lake

level and the risk induced by environmental parameters, including geotechnical conditions. Hence, the wind and wave climate of the lake was studied, and Hydrotam-3D [12] was employed to calculate the combined influence of the wind and wave setup with the storm surge, which affects the lake level. This study focuses mainly on the stability of pipelines trenched/buried in the sea/lakebed by considering the effect of global warming and climate change to incorporate MLL changes in the future.

Figure 1. The ruptured pipeline on the Burdur Lakebed was exposed due to the lake's drying.

2. The Hybrid Hydrodynamic MCS Risk Model

A New Hybrid Hydrodynamic Monte Carlo Simulation (HMCS) Model for the design of maritime structures is presented. The model is implemented in the pipeline project of Burdur Lake by incorporating various sub-models to consider the critical environmental conditions at the limit state, such as wind, waves, current, storms, and climate change. These variables are modeled by the three-dimensional hydrodynamic model Hydrotam-3D [3,12,13].

The developed Hybrid 3D Hydrodynamic Monte Carlo Simulation (HMCS) model represents a significant advancement over existing risk models by incorporating comprehensive environmental factors, utilizing advanced simulation techniques, and explicitly addressing the impacts of climate change. Traditional design codes often follow a deterministic approach, lacking in the comprehensive integration of dynamic environmental factors such as wind, waves, currents, and geotechnical conditions, and may not adequately handle the uncertainties, including the long-term effects of climate change. On the other hand, most countries are developing new design codes to modify the risk levels for climate change's effects, such as sea-level rises, changes in precipitation, or changes in the frequency/intensity of winds/storms/waves in coastal and marine designs.

In contrast, the HMCS model adopts a risk-based design approach, integrating submodels for climate change, wind, waves, current, and geotechnical conditions using the Hydrotam-3D model to simulate interactions between marine structures and environmental parameters, enhancing design reliability. Utilizing MCSs, the HMCS model assesses variability and uncertainty in design parameters, providing robust predictions of pipeline stability under diverse conditions. This holistic climate change approach ensures more sustainable and resilient infrastructure. Advanced simulation techniques combined with the adaptability to dynamic conditions, such as fluctuating lake levels and storm surges, set the HMCS model apart from traditional methods.

The article highlights the practical application of the model in the Burdur Lake Water Pipeline Project, demonstrating its effectiveness in real-world scenarios and capability to address specific environmental challenges, thus ensuring the development of resilient and sustainable maritime infrastructure capable of withstanding future environmental uncertainties.

The Hydrotam-3D model is successfully utilized for various real case projects on the coastline of Türkiye and was verified in studies by [14–18] and [19–22]. The sub-models of Hydrotam-3D are illustrated in Figure 2. The hydrodynamic model uses GIS, which can provide cloud access to the model's functions. The model database contains all data from meteorological stations (MS) and monitored physicochemical data on the field.

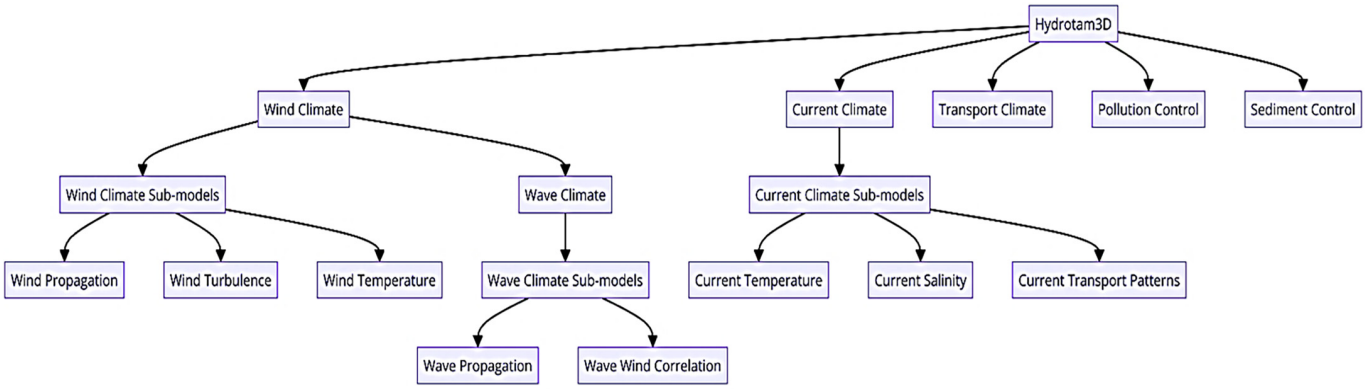

Figure 2. Hydrotam-3D computational sub-models.

The Hybrid 3D Hydrodynamic Transport Coupled Monte Carlo Simulation (HMCS) Model includes six sub-models: Climate Change, Wind Climate, Wave Climate, Current Climate, Geotechnical, and Monte Carlo Risk sub-models. The flow chart belongs to the modeling process presented in Figure 3.

Hydrotam-3D is the core model that integrates various environmental factors. Within its framework, the Wind Climate sub-model includes hourly wind data from Turkish Meteorological Stations, 6-h wind data from the ECMWF (European Centre for Medium-Range Weather Forecasts) Operational archive with a 0.10° horizontal resolution, ERA (ECMWF Re-analysis) Interim data with a 0.25° horizontal resolution, and NCEP (National Center for Atmospheric Prediction) CFSR (Climate Forecast System Reanalysis) data with a 0.50° horizontal resolution [23]. Data from this sub-model, supply the Wave Climate model, impacting wave formation and behavior. The Wave Climate sub-model includes Wave Propagation, which examines wave movement through water influenced by wind and other factors, and Wave Wind Correlation, which studies the relationship between wave patterns and wind conditions. This interaction influences the Current Climate model, which consists of sub-models like Current Temperature, monitoring temperature variations within water currents; Current Salinity, tracking the salt concentration influencing the water density and current behavior; and Current Transport Patterns, analyzing how currents move and distribute substances. The Current Climate model integrates data from the Wave Climate and affects Pollution Control and Transport Climate models. Pollution Control works with the Current Climate to manage and predict the dispersion of pollutants. At the same time, Transport Model studies how currents and climatic conditions impact the transportation of substances and materials in the water. Sediment Control integrates Pollution Control and Transport Model data to manage and predict sediment movement and deposition. Overall, the Wind Climate impacts the Wave Climate by determining wind-driven wave formation; the Wave Climate influences the Current Climate through wave–current interactions; the Current Climate sub-models provide essential data for the Pollution Control and Transport Model, ensuring accurate predictions of pollutant dispersion and material transport; and Pollution Control and Transport Model data feed into Sediment Control, managing sediment dynamics in the aquatic environment.

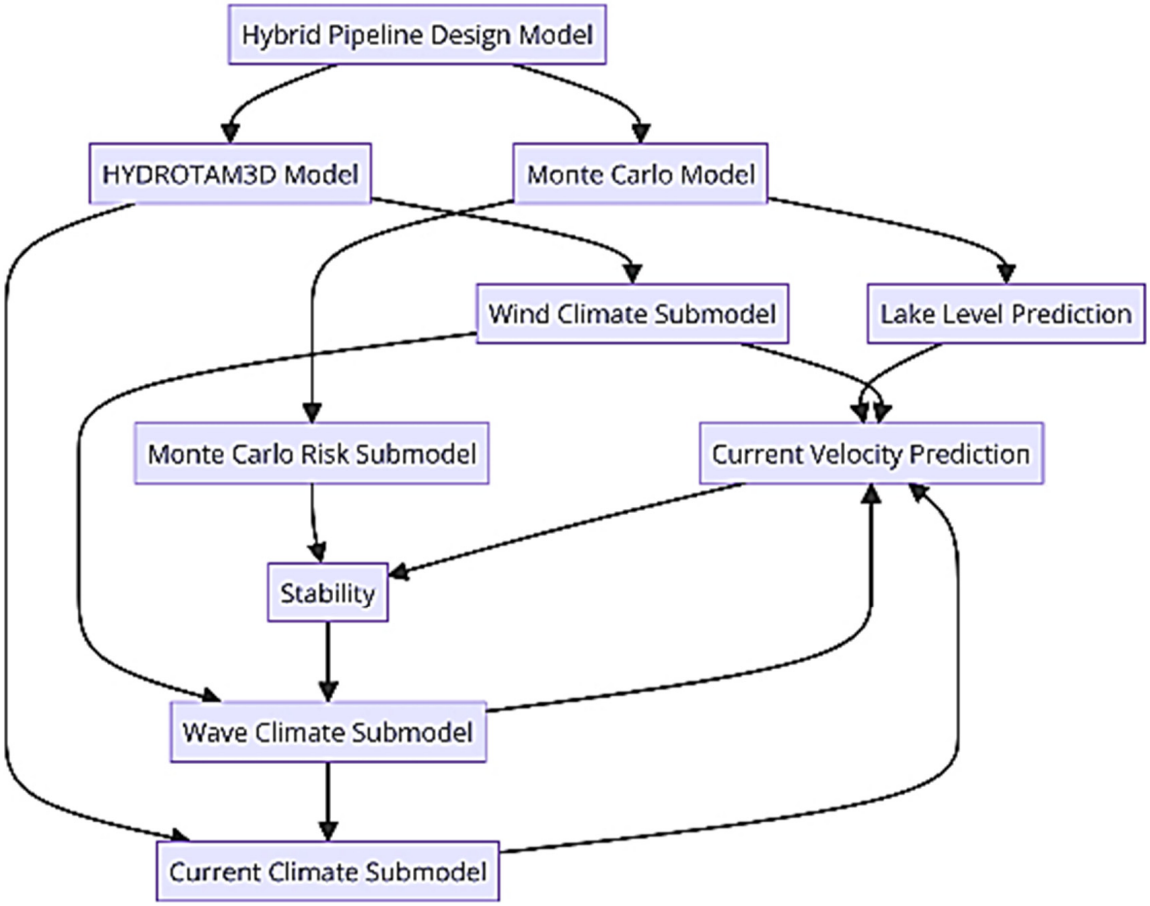

Figure 3. The New Hybrid 3D Hydrodynamic Transport Coupled Monte Carlo Simulation (HMCS) Model Flow Chart.

Hydrotam-3D integrates all these models, ensuring a comprehensive analysis of environmental factors affecting maritime structures. This interconnected system allows for a holistic approach to assessing and managing the impacts of environmental changes on maritime structures, particularly under the influence of climate change.

The Climate Change Sub-model includes lake-level predictions of the RCP8.5 climate change scenario to determine water levels for the pipeline design. The Coupled Model Intercomparison Project Phase 6 (CMIP6) is used to obtain the effect of climate change, and the results of the 2041–2060 and 2081–2100 periods were considered for the Monte Carlo module [24].

The Wind Climate Sub-model handles extreme and long-term statistics for all MS and ECMWF wind data [23] by six-hour intervals covering Turkish coastal waters from 2000 to 2022. The model provides the wind roses for annual, seasonal, and monthly time steps. The highest wind speeds and directions are computed using Fisher Tippet Type I (FTT-1) probability distribution, and the governing wind directions for that location are identified.

The Wave Climate Sub-model gives long-term and extreme wave statistics, yearly and seasonal wave roses, and relations between wave heights and periods by predicting significant wave heights and periods. Wave transformations such as refraction, shoaling, and diffraction equations are based on the velocity potential presented by [25]. The mild slope equation has been separated into three equations using the wave function derived from the velocity potential and considering the approach angle over irregular bathymetries.

Computationally, the numerical model simulates propagation on broad coastal areas under changing wave conditions [16,26]. The complex velocity potential (φ) was given by [25]:

$$\varphi = ae^{is} \quad (1)$$

in which s is the phase function of the wave and a is the amplitude. Equation (1) is used for wave propagation in two plane dimensions, and Equations (2) and (3) are obtained:

$$\frac{1}{a}\left[\frac{\partial^2 a}{\partial x^2}+\frac{\partial^2 a}{\partial y^2}+\frac{1}{CCg}(\nabla a.\nabla(CCg))\right]+k^2-|\nabla s|^2=0 \quad (2)$$

$$\frac{1}{a}\left[\frac{\partial^2 a}{\partial x^2}+\frac{\partial^2 a}{\partial y^2}+\frac{1}{CCg}(\nabla a.\nabla(CCg))\right]+k^2-|\nabla s|^2=0 \quad (3)$$

$$\nabla\cdot\left(a^2 CC_g\nabla s\right)=0 \quad (4)$$

in which C is the wave celerity, C_g is the group velocity, k is the wave number and ∇ is the gradient. The Equations (4)–(6) are solved to obtain the wave height H, propagation angle θ, and gradient of the phase function ∇s:

$$|\nabla s|=\mathrm{k}^2+\frac{1}{H}\left[\frac{\partial^2 H}{\partial x^2}+\frac{\partial^2 H}{\partial y^2}+\frac{1}{CCg}\left[\frac{\partial H}{\partial x}\frac{\partial CCg}{\partial x}+\frac{\partial H}{\partial y}\frac{\partial CCg}{\partial y}\right]\right] \quad (5)$$

$$\frac{\partial}{\partial x}\left(H^2 CCg|\nabla s|cos\theta\right)+\frac{\partial}{\partial y}\left(H^2 CCg|\nabla s|sin\theta\right)=0 \quad (6)$$

The significant breaker depth ($h_{1/3}$) and the significant breaker height ($H_{1/3}$) for the unidirectional random waves are calculated by using the Goda Method [27], as given in Equations (7)–(9). The wave setup, including the effect of surface rollers, is calculated by Equations (10) and (11). The dynamic wave setup (surf beat) is obtained from Equation (12) at the shoreline for these wave conditions.

$$\left(\frac{H_{\frac{1}{3},peak}}{h_{\frac{1}{3},peak}}\right)_h=\frac{A}{h/L_0}\left\{1-\exp\left[-1.5\,\pi\frac{h}{L_0}\left(1+11s^{4/3}\right)\right]\right\} \quad : \quad A=0.12 \quad (7)$$

$$H_{1/3}=\begin{cases} K_s H_0', & : h/L_0<0.2 \\ min\{(\beta_0 H_0'+\beta_1 h),\beta_{max}H_0', K_s H_0'\} & : h/L_0<0.2 \end{cases} \quad (8)$$

$$H_{max}=H_{250}=\begin{cases} 1.8K_s H_0', & : h/L_0<0.2 \\ min\{(\beta_0 H_0'+\beta_1 h),\beta_{max}H_0', 1.8K_s H_0'\} & : h/L_0<0.2 \end{cases} \quad (9)$$

Significant Wave Height $H_{1/3}$	**Maximum Wave Height H_{max}**
$\beta_0=\left(H_0'/L_0\right)^{-0.38}0.028\,exp[20s^{1.5}]$	$\beta_0^*=0.052\left(H_0'/L_0\right)^{-0.38}exp[20s^{1.5}]$
$\beta_1=0.52\exp[2.4\,s]$	$\beta_1^*=0.63\exp[3.8\,s]$
$\beta_{max}=max\left\{0.92,\ 0.32\left(H_0'/L_0\right)^{-0.29}exp[2.4\,s]\right\}$	$\beta_{max}^*=max\left\{1.65,\ 0.53\left(H_0'/L_0\right)^{-0.29}exp[2.4\,s]\right\}$

Including the effect of surface rollers:

$$\zeta_{\theta_{0=0}}/H_0=(0.0063+0.768\,s)-(0.0083+0.011\,s)\ln H_0/L_0+(0.00372+0.0148s)\left[\ln H_0/L_0\right]^2 \quad (10)$$

$$\zeta=\zeta_{\theta_{0=0}}(\cos\theta_0)^{\,0.545+0.038\ln H_0/L_0} \quad (11)$$

and for oblique wave incidence:

$$\zeta_{rms}=\frac{0.04\,(\eta_{rms})_0}{\sqrt{\frac{H_0'}{L_0}\left(1+\frac{h}{H_0'}\right)}}=\frac{0.01H_0'}{\sqrt{\frac{H_0'}{L_0}\left(1+\frac{h}{H_0'}\right)}} \quad (12)$$

The Current Climate Sub-model provides the 3D modeling of currents under the effect of wind, density stratification, tides, and storm surges. The Hydrodynamic Sub-model applies a 3D k-ε model for turbulence. The governing equations in the three-dimensional Cartesian coordinate system are given in Equations (13)–(16):

The continuity equation:

$$\frac{\partial w}{\partial z} + \frac{\partial u}{\partial x} + \frac{\partial v}{\partial y} = 0 \tag{13}$$

The momentum equations for x and y:

$$\frac{\partial u}{\partial t} + u\frac{\partial u}{\partial x} + v\frac{\partial u}{\partial y} + w\frac{\partial u}{\partial z} = fv - \frac{1}{\rho_0}\frac{\partial p}{\partial x} + 2\frac{\partial}{\partial x}\left(v_X\frac{\partial u}{\partial x}\right) + \frac{\partial}{\partial y}\left(v_y\left(\frac{\partial u}{\partial y} + \frac{\partial v}{\partial x}\right)\right) + \frac{\partial}{\partial z}\left(v_y\left(\frac{\partial u}{\partial z} + \frac{\partial w}{\partial x}\right)\right) \tag{14}$$

$$\frac{\partial u}{\partial t} + u\frac{\partial u}{\partial x} + v\frac{\partial u}{\partial y} + w\frac{\partial u}{\partial z} = fv - \frac{1}{\rho_0}\frac{\partial p}{\partial x} + 2\frac{\partial}{\partial x}\left(v_X\frac{\partial u}{\partial x}\right) + \frac{\partial}{\partial y}\left(v_y\left(\frac{\partial u}{\partial y} + \frac{\partial v}{\partial x}\right)\right) + \frac{\partial}{\partial z}\left(v_y\left(\frac{\partial u}{\partial z} + \frac{\partial w}{\partial x}\right)\right) \tag{15}$$

and in the vertical direction z:

$$\frac{\partial w}{\partial t} + u\frac{\partial w}{\partial x} + v\frac{\partial w}{\partial y} + w\frac{\partial w}{\partial z} = -\frac{1}{\rho_0}\frac{\partial p}{\partial z} + gz + \frac{\partial}{\partial x}\left(v_x\left(\frac{\partial w}{\partial x} + \frac{\partial u}{\partial z}\right)\right) + \frac{\partial}{\partial y}\left(v_y\frac{\partial w}{\partial y} + \frac{\partial v}{\partial z}\right) + 2\frac{\partial}{\partial z}\left(v_z\frac{\partial w}{\partial z}\right) \tag{16}$$

where ν_x, ν_y, and ν_z are the eddy viscosities in the x, y, and z directions, respectively; p = pressure; f is the Coriolis coefficient; g is the gravitational acceleration; $\rho(x,y,z,t)$ is the water density, and ρ_0 is the density of the reference value.

The lake density changes according to its salinity, temperature, and pressure. Its distribution depends on the distribution of the temperature and salinity. The variable σ_t can be defined as a function of density ρ as:

$$\sigma_t = (\rho - 1) \times 10^3 \tag{17}$$

where ρ is the density in $\mathrm{gr/cm^3}$. The following equations are used to determine the density as a function of temperature and salinity:

$$C = 999.83 + 5.053d - 0.048d^2 \tag{18}$$

$$\beta = 0.808 - 0.0085d \tag{19}$$

$$\alpha = 0.0708(1 + 0.351d + 0.068(1 - 0.0683d)T) \tag{20}$$

$$\gamma = 0.003(1 - 0.059d - 0.012(1 - 0.064d)T) \tag{21}$$

$$\rho = C(d) + \beta(d)S - \alpha(T,d)T - \gamma(T,d)(35 - S)T \tag{22}$$

where T is the temperature (°C), S is the salinity (‰), and d is the water depth (km).

The following diffusion equations are used in the model:

$$\frac{\partial T}{\partial t} + u\frac{\partial T}{\partial x} + v\frac{\partial T}{\partial y} + w\frac{\partial T}{\partial z} = \frac{\partial}{\partial x}\left(D_x\frac{\partial T}{\partial x}\right) + \frac{\partial}{\partial x}\left(D_y\frac{\partial T}{\partial y}\right) + \frac{\partial}{\partial z}\left(D_z\frac{\partial T}{\partial z}\right) \tag{23}$$

where T is the temperature and D_x, D_y, and D_z are the diffusion coefficients of turbulence. The same equation is valid for salinity (S).

The Geotechnical Sub-model enables the inclusion of the necessary geotechnical parameters and soil property variability in the stability calculations of the water transmission pipe system. For the problem under consideration, the design values and the uncertainty of the unit weight and the soil shear strength are to be estimated. For this purpose, the results from the site investigation were examined thoroughly to determine the mean values of design parameters.

Geotechnical variability is complex and results from inherent soil variability, measurement error, and transformation uncertainty (e.g., [28]). Of those, inherent soil variability

occurs due to naturally occurring geologic procedures that form the soil. The next source is the measurement error, which results from equipment and random testing effects [29]. When considered together, these two sources are named the data scatter. It should be considered that field surveying is affected by statistical unpredicted or sampling flaws, which is the result of delimited information that can be reduced to a minimum by increasing the number of tests; however, measurement errors will increase this time [28]. As a result, design soil properties are commonly obtained using empirical or correlation-based models applied to field or laboratory measurements, but this process introduces transformation uncertainty into the calculations. The overall uncertainty of any design geotechnical property should be systematically determined considering the relative contribution of these three sources based on the quality of the tools, the control of the procedure, and the accuracy that belongs to a specific correlation model as a minimum.

The following probabilistic method can be persistently utilized to integrate the immanent soil variability, measurement error, and transformation uncertainty ([30]: it can be accepted that the following probabilistic transformation model parameter of design (ξ_d) is obtained out of the possession of test measurement (ξ_m).

$$\xi_d = T(\xi_m, \varepsilon) \tag{24}$$

in which $T(\cdot)$ is the transformation function, ε is the uncertainty of the model, (w) represents inherent soil variability, and (e) represents the measurement error. These are added to Equation (21), which is exchanged to Equation (22) for the measured soil property, ξ_m:

$$\xi_m(z) = t(z) + w(z) + e(z) \tag{25}$$

in which t is the deterministic trend, w is the inherent variability, and e is the measurement error. w and e, which are undetermined parameters, are considered uncorrelated; hence, the derived sources are independent. Refs. [28,30]. Thus, the design parameter is defined as:

$$\xi d = T(t + w + e, \varepsilon) \tag{26}$$

Here, the mean of w, e, and ε is zero.

Equation (23) can be linearized for the mean of (w, e, ε) by using the Taylor series expansion [31]:

$$\xi d \approx T(t,0) + w\ \partial T/\partial w\,|_{(t,0)} + e\ \partial T/\partial e\,|_{(t,0)} + \varepsilon\ \partial T/\partial \varepsilon\,|_{(t,0)} \tag{27}$$

The mean and variance values of ξd have been determined with the aid of implementing second-moment probabilistic methods to Equation (23) [31]:

$$m_{\xi d} \approx T(t,0) \tag{28}$$

$$s_{\xi d}{}^2 \approx [\partial T/\partial w\,|_{(t,0)}]^2 s_w{}^2 + [\partial T/\partial e\,|_{(t,0)}]^2 s_e{}^2 + [\partial T/\partial \varepsilon\,|_{(t,0)}]^2 s_\varepsilon{}^2 \tag{29}$$

$m_{\xi d}$ and $s_{\xi d}{}^2$ are the mean and variance of ξ_d, respectively, $s_w{}^2$ is the variance of the inherent soil variability, $s_e{}^2$ is the variance of the measurement error, and $s_\varepsilon{}^2$ is the variance of model uncertainty.

Equation (26) calculates the general mean and variance, i.e., the second-moment statistics, which belong to design characteristics at a point in the soil mass. However, the spatial average of the design parameter over the influence depth is usually required for the geotechnical design. If t and $\partial T/\partial w$ (or $\partial \xi_d/\partial w$) represent constant values, the mean of the spatial average is identical to the presented data within Equation (25). In contrast, the variance of the spatial average ($s_{\xi a}{}^2$) has been presented in Equation (27) [32]:

$$s_{\xi a}{}^2 \approx [\partial T/\partial w\,|_{(t,0)}]^2\ \Gamma^2(L_a)\ s_w{}^2 + [\partial T/\partial e\,|_{(t,0)}]^2 s_e{}^2 + [\partial T/\partial \varepsilon\,|_{(t,0)}]^2 s_\varepsilon{}^2 \tag{30}$$

where $\Gamma^2(\cdot)$ is the variance reduction function based on the averaging interval length, L_a. [32] presented an approximate variance reduction function for practical implementations in the following:

$$\Gamma^2(L_a) = 1 \text{ for } L_a \leq \delta_v \quad (31)$$

$$\Gamma^2(L_a) = \delta_v / L_a \text{ for } L_a > \delta_v \quad (32)$$

in which δ_v is the vertical scale of fluctuation.

The general probabilistic approach is implemented to obtain the typical second-moment statistics of the unit weight and undrained shear strength of Burdur Lake soil where the water transmission pipeline is found.

The Monte Carlo Risk Sub-model: This sub-model presents the development of a statistical Monte Carlo Risk Sub-model for conducting the stability analyses of pipelines to assess the failure probability of buried pipelines through a comprehensive risk assessment approach. The sub-model can simulate the vertical stability failure function to understand the factors leading to pipeline system failures, such as the soil type, burial depth, pipeline diameter, and external loads. The conclusions provided by the simulation give a statistical distribution of failure probabilities, which are used to forecast the failure risk under different environmental circumstances.

The scientific modeling aspect of the Hybrid 3D Hydrodynamic Monte Carlo Simulation (HMCS) model is characterized by its integration of multi-dimensional environmental sub-models and advanced probabilistic techniques.

The HMCS model employs the Hydrotam-3D framework, which encompasses detailed sub-models for wind, wave, current, and geotechnical conditions, providing a comprehensive simulation environment. These sub-models are interconnected to capture the dynamic interactions between various environmental factors and marine structures. The wind climate sub-models, for instance, account for wind propagation, turbulence, and temperature, feeding data into the wave climate sub-models that examine wave propagation and wind–wave correlations. This hierarchical structure continues with the current climate sub-models, which monitor temperature, salinity, and transport patterns within water currents. The model also incorporates geotechnical sub-models that address soil variability and strength, which is critical for assessing the stability of submarine pipelines.

A significant innovation in the HMCS model is its use of MCSs to manage the inherent uncertainties and variabilities in environmental conditions. By generating thousands of possible scenarios, the model provides robust statistical predictions of pipeline stability, accounting for fluctuating lake levels, storm surges, and a changing wave climate due to climate change. The probabilistic nature of the Monte Carlo approach allows for a detailed sensitivity analysis, identifying which parameters most significantly impact the model's outputs. The sensitivity study enables the refinement of the model and enhances its predictive reliability. Furthermore, the model's ability to simulate complex interactions and adapt to dynamic environmental conditions underscores its advanced computational capabilities, making it a valuable tool for designing resilient and sustainable maritime infrastructure.

The modeling aspects of the Hybrid 3D Hydrodynamic Monte Carlo Simulation (HMCS) model demonstrate significant advancements over solely simulation-based approaches. Traditional simulations often focus on specific aspects or single environmental factors without fully integrating the wide range of variables that can impact the stability and resilience of maritime structures. In contrast, the HMCS model's comprehensive integration of multi-dimensional environmental sub-models provides a holistic understanding of the interactions between wind, wave, current, and geotechnical conditions.

While standard simulations might isolate variables such as wave heights or current velocities, the HMCS model captures the interconnected nature of these factors through its hierarchical sub-model structure. For example, the wind climate sub-models inform the wave climate sub-models, which influence the current climate sub-models, creating a dynamic feedback loop that better represents real-world conditions. This level of integration

is crucial for accurately predicting the impacts of complex environmental changes, such as those induced by climate change.

Additionally, the HMCS model employs MCSs to manage uncertainties and variabilities, a significant improvement over the deterministic method. By generating thousands of possible scenarios, the Monte Carlo approach provides robust statistical predictions and enables detailed sensitivity analysis, identifying the most critical parameters affecting pipeline stability. This probabilistic method contrasts with the fixed-output nature of traditional simulations, offering a more nuanced understanding of risk and reliability.

In summary, while solely given simulations provide valuable insights into specific environmental conditions, the HMCS model's comprehensive and probabilistic approach ensures a more accurate, reliable, and holistic analysis of maritime infrastructure design. It enhances the predictive capability by considering the full spectrum of interacting environmental factors and their uncertainties. The model offers a more resilient and sustainable design solution for submarine pipelines and other marine structures.

3. Case Study of Burdur Lake Water Transmission System

The tectonic Burdur Lake is located between the provinces of Burdur and Isparta in the southwest region of Türkiye. Regarding the surface area, the lake is the seventh largest in Türkiye (Figures 4 and 5).

Since the well reservoir and pumping station are on opposite sides of the lake, drinking water must be drawn across the lake to service the city of Burdur, as the drinking water pipeline system can operate safely during the climate change era.

In that case, Burdur will not face a water shortage in the next few decades as the city's population continuously increases [33]. A Burdur Lake pipeline case study indicates the pertinency of the suggested hybrid model. The pipeline had initially been installed in the deep-water region of the lake; however, the decline in the water level caused by climate change resulted in the pipeline's exposure to breaking waves. Climate change led to merging the increased intensity of the storms and the breaking of waves, which later failed in the pipeline. Considering such environmental factors, along with dynamic conditions, is essential during the design concerning the integrity and reliability of the pipeline. The proposed hybrid model sets the baseline for assessing the safety and reliability of submarine pipelines under dynamic environmental conditions. This paper shows how climate change will affect the water pipeline system that has already been installed in the bed of Burdur Lake and designed under deep water conditions. However, the pipeline showed up in the breaking zone due to the gradual falling of the water level. The pipeline has, therefore, exposed the effect of breaking waves coupled with the increase in the strength of storms affecting this region, which has resulted in its rupture. The rise in storm intensity is also attributed to climate change, which has eventually led to the breakup of the pipeline, as illustrated in Figure 6.

The static conditions for which the pipeline was designed were no longer maintained, leading to its failure. Furthermore, the consequences of climate change have led to the transformation of the parts of the Burdur Lake region from a hydrologically active environment to a terrestrial arid zone. This transformation has further exacerbated the negative impact of the failure of the water pipeline system. Consequently, a new project considering all these environmental factors affected by climate change has become necessary. Based on these considerations, the present study highlights the need for the cautious reflection of global warming on hydrological systems and infrastructure, particularly in districts prone to extreme weather conditions, focusing specifically on the Burdur Lake region as a significant example.

Following the rupture of the first pipeline system, a new pipeline system under the lakebed has been designed. This design feature will shelter the pipeline system from future climate change and meteorological effects if the lake resumes losing its surface area due to global warming. The new pipeline system will be constructed on the lakebed with 8.00 m of water depth in Burdur Lake.

Figure 4. Location of Burdur Lake [34].

Figure 5. Areal map of Burdur Lake [34].

Figure 6. The broken part of the former Burdur Lake pipeline is in the dried zone of the lake.

3.1. Climate Change Sub-Model

In Climate Projections with New Scenarios for the Türkiye project, the RCP8.5 scenario of three different model data was obtained from Ref [35]. The average annual temperature rise for 2016–2040 in Türkiye is expected to vary between 1 °C and 2 °C based on three GCMs (HadGEM2-ES, MPI-ESM-MR, and GFDL-ESM2M). In 2041–2070, the increase in the surface temperature is expected to vary between 1.5 °C and 4 °C. In the last period (2071–2099), the average annual temperature rising is expected to vary between 1.5 °C and 5 °C. The increase would be higher in winter for inner regions (Figure 7). For Burdur Lake, the increase will be around 1.5 °C in the first period, and it is predicted to rise to 2 °C in 2041–2070 and above 3.5 °C in 2071–2099. Additionally, when precipitation projections are examined, total precipitation is predicted to decrease in all periods throughout the Burdur basin, with a maximum predicted decrease of 30%. The predicted lake levels according to the region's global warming scenarios from the CMIP6 model were obtained from the Effect of Climate Change on Water Resources Project [36], and these mean predictions were simulated by an MCS using the variations given by the [35]. The predicted lake levels were compared for the years 1986 and 2020 since Burdur Lake experienced a dramatic decrease in terms of surface area, as analyzed by [37].

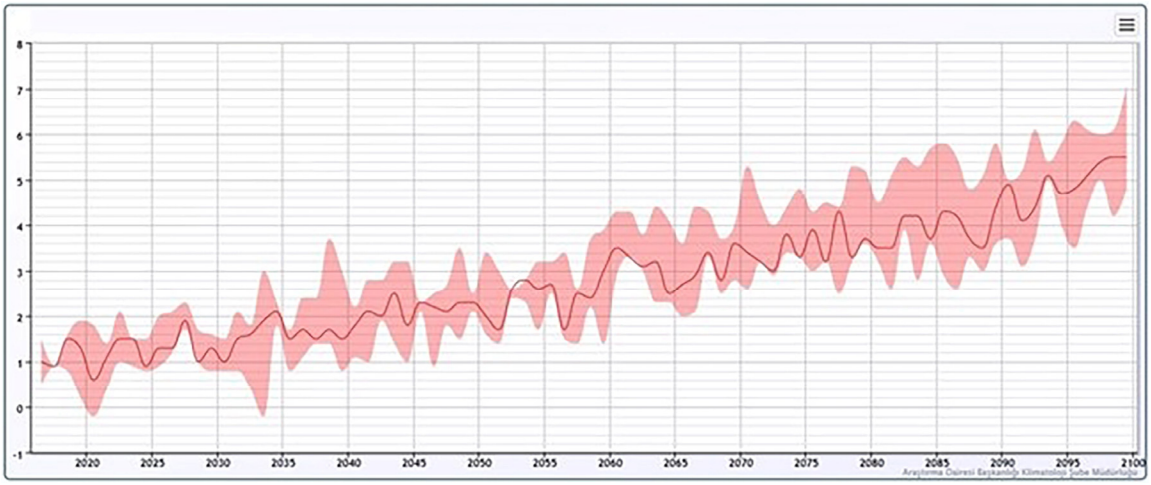

Figure 7. According to RCP8.5, projections of Türkiye's annual average temperature anomaly range [38].

While the water surface area of Burdur Lake was 206 km^2 in 1986, this area decreased to 125 km^2 in 2019. Consequently, Burdur Lake has recently lost approximately 40% of its total surface area and dried up. The ruptured pipeline area is now in the dried part of the lake. The decline in the surface area of Burdur Lake is one of the most obvious examples of the effects of the global warming era. The lake had a maximum water level (857.5 m from sea datum) in 1970 with a surface area of 215.7 km^2 and a volume of 6.826 hm^3 (Figure 8). The part of the bathymetry for the pipeline is illustrated in Figure 9, and the variation in the lake area (1984–2019) is shown in Figure 10. With the aid of this trend, the MCS sub-model simulates the MLL decrease in the future, and the variation in the average depth considering global warming is obtained from an MCS, as illustrated in Figure 11 [39].

The MCS sub-model analyzed the decreasing trend in MLL, and the distribution attained to MLL was obtained as given in Figure 10. The average water level at the construction depth was 8.50 m in 2023. By simulating the variation in future years, the MLL was estimated to decrease by −53 cm in the next 100 years at the construction depth of the pipeline with a confidence level of 90% (Figure 11). Hence, the pipeline stability was simulated for a depth of 8.5 m by considering the water level decrease in the next 100 years. The MCS was conducted using the results obtained from the Hydrotam 3D model, as indicated in Figure 3, from which the wind, wave setup, and storm surge were computed.

Hence, all these sub-models are related to the MCS to predict the change in the water level of Burdur Lake in the climate change era.

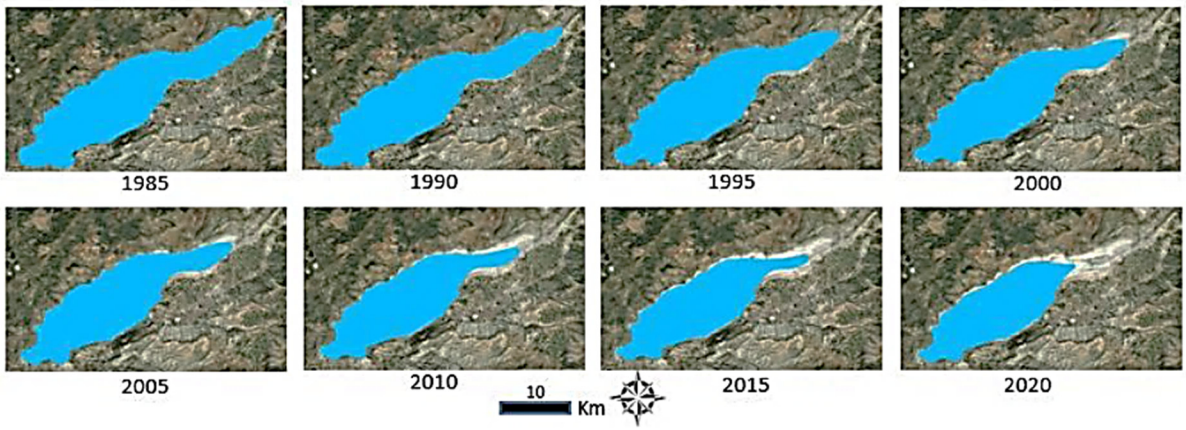

Figure 8. Burdur Lake's surface area has changed over the years [37].

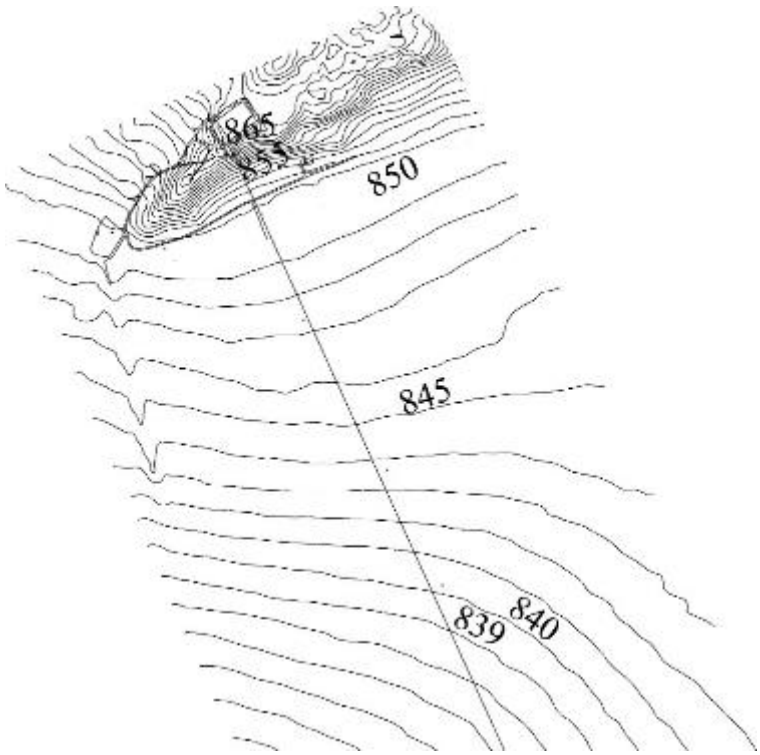

Figure 9. The part of the lake bathymetry and the pipeline (line).

The mean values of the wind and wave setup, storm surge, and their variations were obtained from the Hydrotam 3D model to modify the mean water levels predicted by the region's global warming scenarios obtained from the CMIP6 model and downscaled to Burdur Lake by the Effect of Climate Change on Water Resources Project [36] in the MCS.

The records from Yazıköy station (station no: D10M007), operated by the General Directorate of State Hydraulic Works (DSI), were utilized to validate the simulation ranges. This station records the average lake level from 1969 to 2018. Until 1971, there were no sudden decreases in lake levels. However, between 1971 and 1977, the levels declined, corresponding with a dry period. From 1977 to 1985, the lake levels rose and fluctuated seasonally during a wet period. After 1985, the lake level significantly decreased, independent of dry or wet seasons, except for short-term increases during wet periods. The difference

between the lake's maximum water level (May 1970) and minimum water level (September 2018) is approximately 17 m [40].

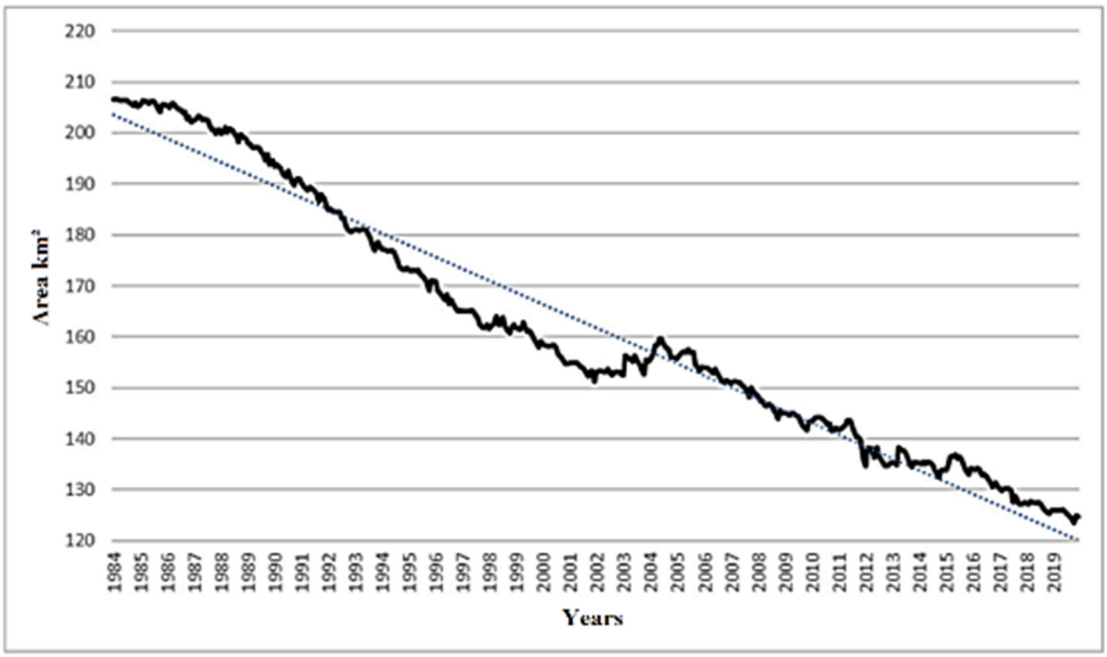

Figure 10. The trend (dotted line) and temporal variation (black line) in the lake area between 1984 and 2019 [39].

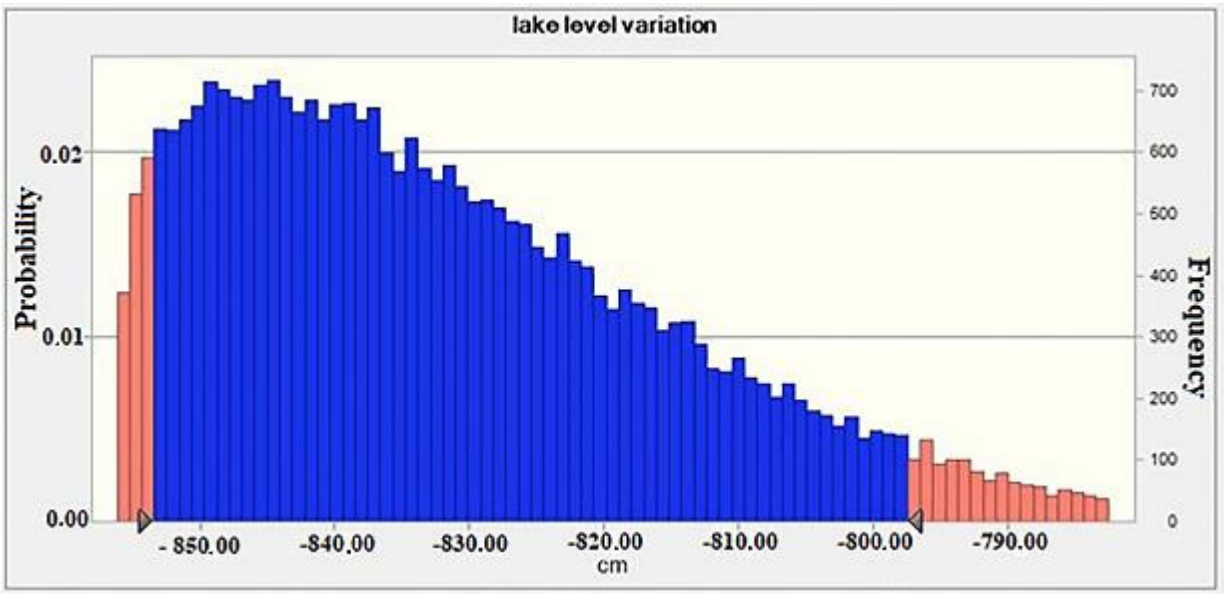

Figure 11. The lake level variation at the construction depth (cm) by MCS.

Hence, all these sub-models are related to the MCS to predict the change in the water level of Burdur Lake in the climate change era. The mean values of the wind, wave setup, storm surge, and variations were obtained from the Hydrotam 3D model to modify the mean water levels predicted by the region's global warming scenarios obtained from the CMIP6 model and downscaled to Burdur Lake by the Effect of Climate Change on Water Resources Project [36] in the MCS.

3.2. Wind Climate Sub-Model

The operational archive 6-h wind forecasts for 2000–2022 of the European Medium-Scale Weather Forecasting Center (ECMWF) and the numerical model wind forecasts from the ECMWF-ERA5 were used [23]. The data for the lake at the coordinates 37.8° N–30.3° E were examined, as shown in Figure 12. Wind sources are compared in Figure 13, and the wind roses are illustrated in Figure 14.

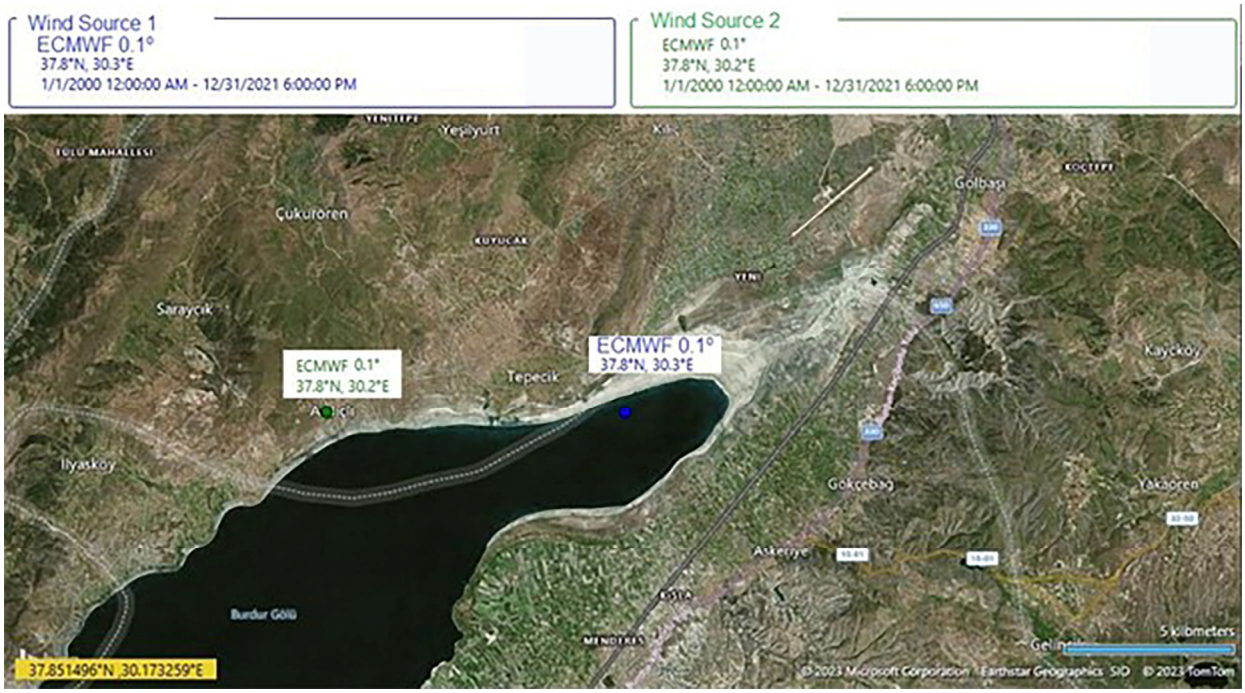

Figure 12. Coordinates for ECMWF Wind Data Sources [12,23].

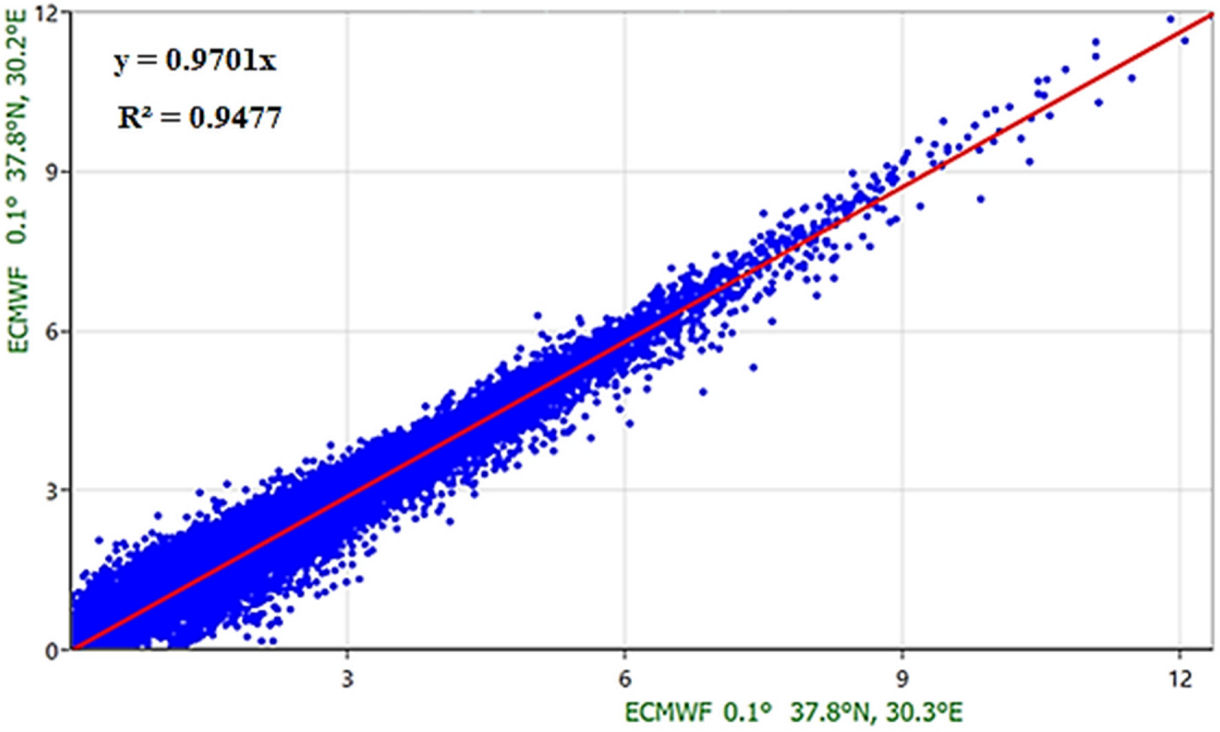

Figure 13. Comparison of wind sources for 37.8° N 30.2° E and 37.8° N 30.3° E wind sources on the lake between 2000 and 2022 [12].

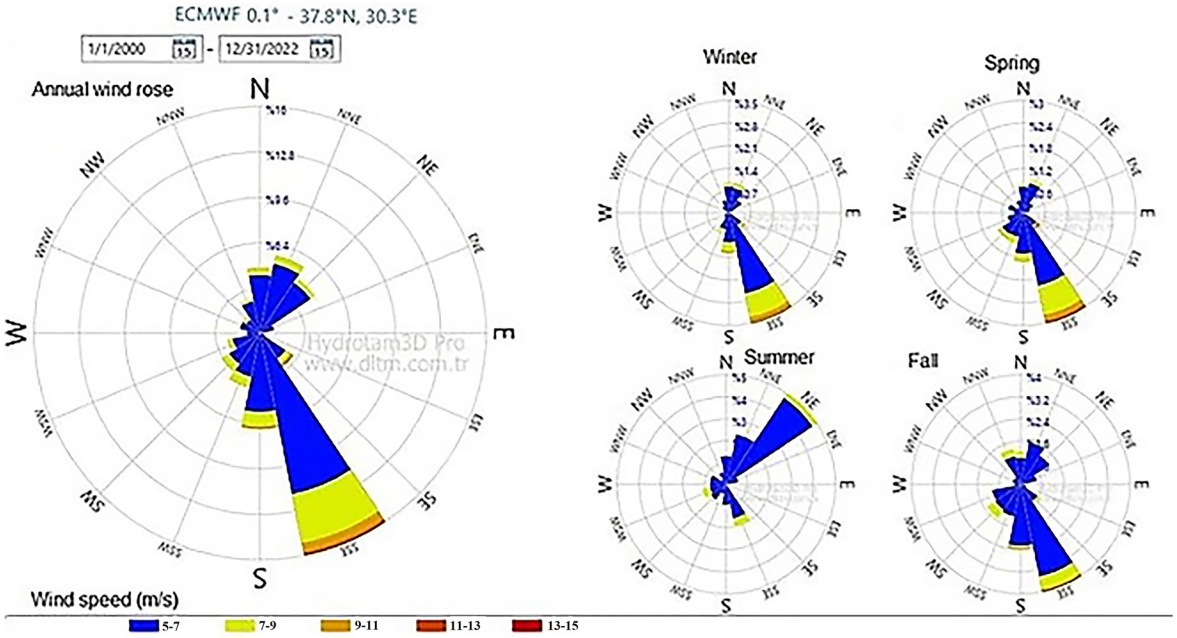

Figure 14. Annual and seasonal wind roses between 2000 and 2022 [12].

As a result, the 37.8° N–30.2° E and 37.8° N–30.3° E operational archive data sources over the lake were compatible with each other, as shown in Figure 13. There is a 2% probability of exceeding the 7 m/s wind speed for the WSW direction, which is the direction with the highest fetch. From the extreme value statistics, the wind speed with a return period of 50 years is obtained as 14 m/s. The Extreme value FFT-1 distribution wind statistics for ECMWF data of 2000–2022 are presented in Figure 15.

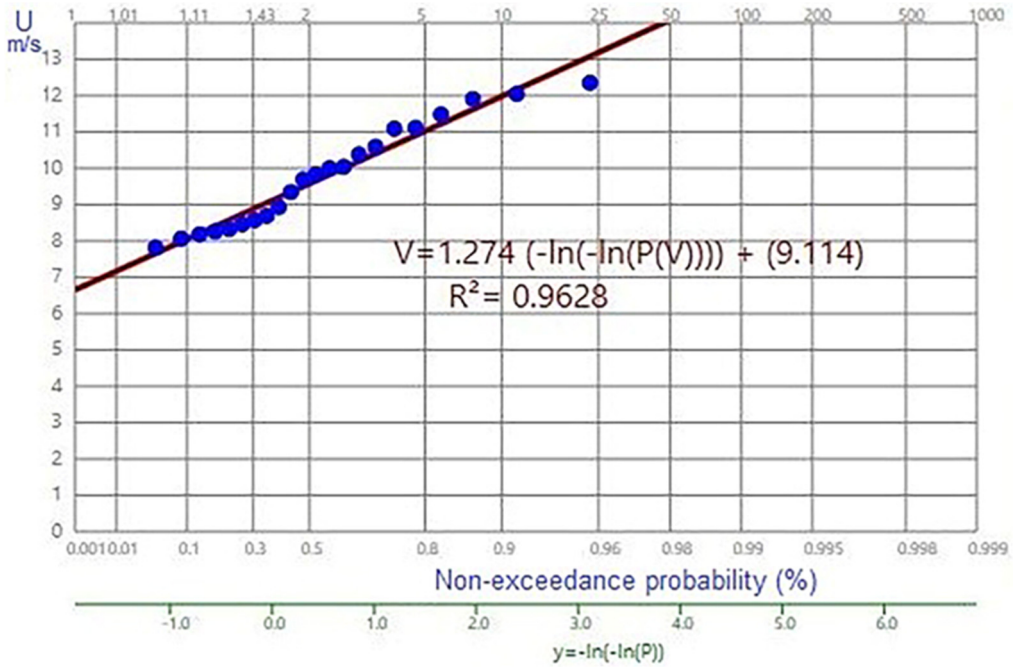

Figure 15. Extreme value distribution wind speed (U m/s) over the lake for 2000–2022 [12].

3.3. Wave Climate Sub-Model

Effective fetch distances (length of the storm area) were obtained as shown on Figure 16, which is 20 km. Due to the geographical position of the lake, the main fetch distance that can cause the maximum storm surge is the West–West Southwest (W-WSW) direction

segment. The parametric spectrum wave prediction model CEM [41] and the numerical model wind forecasts from the ECMWF-ERA5 are utilized in wave climate studies. The fetch distances from the point of concern to the land in all directions are calculated by the HYDROTAM-3D model system [42].

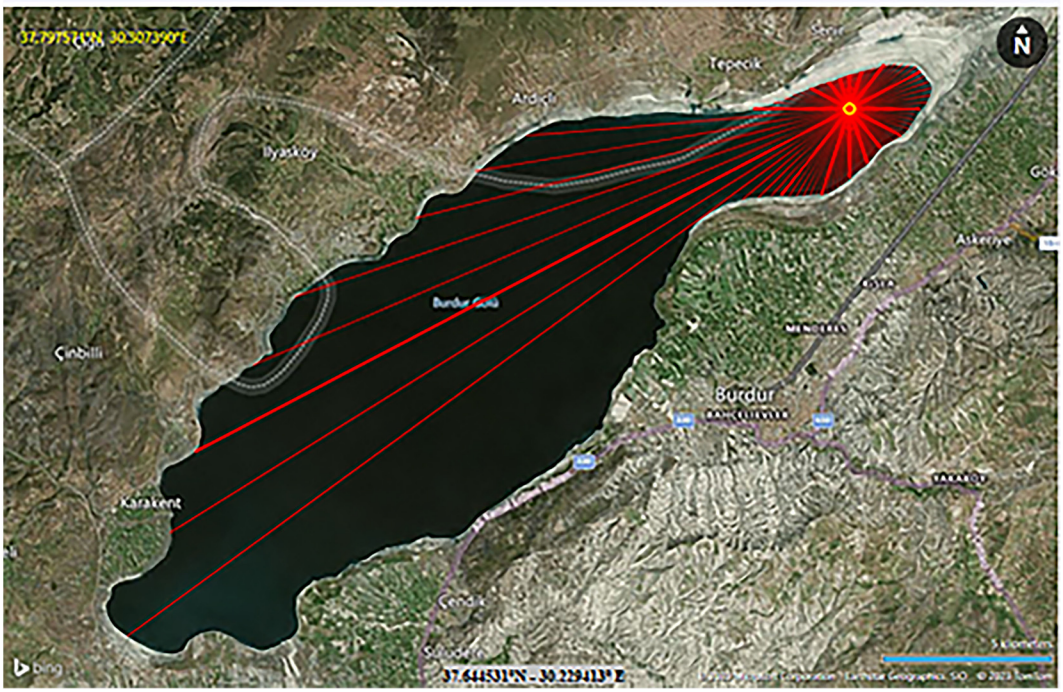

Figure 16. Effective fetch distances for wave directions of the project area.

In the fetch sub-module, the cosine average method is applied to determine the effective wave fetch length in all major directions at angles of θ = 3.75 degrees within a ±22.5-degree range [15]. The duration of wind speed is equal to the number of preceding consecutive and acceptable hours for which the wind speed and direction variations do not exceed 2.5 m/s and a certain value of 15° from the mean, respectively. Corresponding wind speeds and fetch lengths were determined by taking the mean values over this duration using ECMWF-ERA5 archives from 1 January 2000 to 31 December 2021 for the coordinates of 37.8°N 30.3°E; hence, only wind was used as the input. Ref. [43] investigated the performance of ANFIS and CEM methods for predicting the wave parameters in fetch-limited conditions for Lake Ontario. They found that the CEM [41] method overestimates the significant wave height, leaving the designer safe.

In the HYDROTAM-3D modeling database, wind prediction results for the 2000–2021 period at six-hour intervals from the ECMWF-ERA5 archives for each point on the horizontal resolution grid of 0.1° covering the Turkish land and marine area were recorded. Using the CEM parametric wave model [41] based on wind directional predictions, the "long-term" and "extreme value" statistics of deep-sea significant wave heights are studied [44]. Long-term wave statistics include temporally continuous data. For the statistical evaluation of wave heights, the Log-normal distribution shows the relationship between the significant wave heights and their occurrence probabilities. Annual wave roses show significant wave heights in each direction throughout the year. The directional segments indicating where the waves come from are selected to be the same as the geographical directions. The extreme value statistics for significant wave heights have also been applied. The annual maximum values of significant wave heights are assumed to follow the FFT-1 (Gumbel) distribution. The best-fit line for the values is drawn using linear regression analysis and extended beyond the duration covered by the data [44].

The annual and seasonal wave roses of Burdur Lake are given in Figure 17. It is seen that waves mostly occur in the SSW-WSW directional range, which has the highest fetch

length. The extreme value FTT-1 distribution was determined from the long-term wave statistics as presented in Figure 18. The design of the significant wave height with a return period of Tr = 100 years in the lake is estimated at Hs = 1.2 m using the wave climate sub-model.

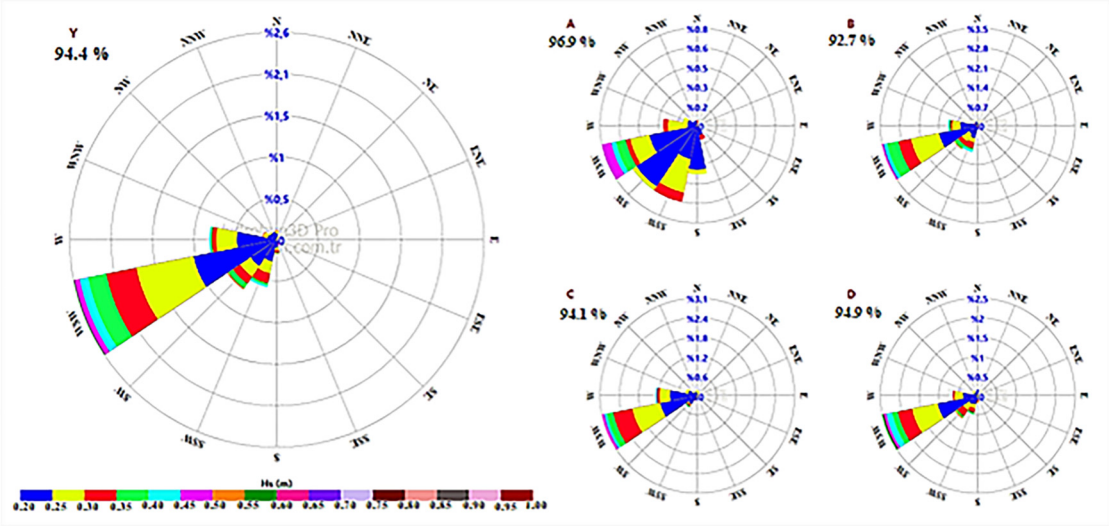

Figure 17. Burdur Lake Annual (**Y**) and Seasonal Wave Roses: (**A**) Winter, (**B**) Spring, (**C**) Summer, and (**D**) Autumn [12].

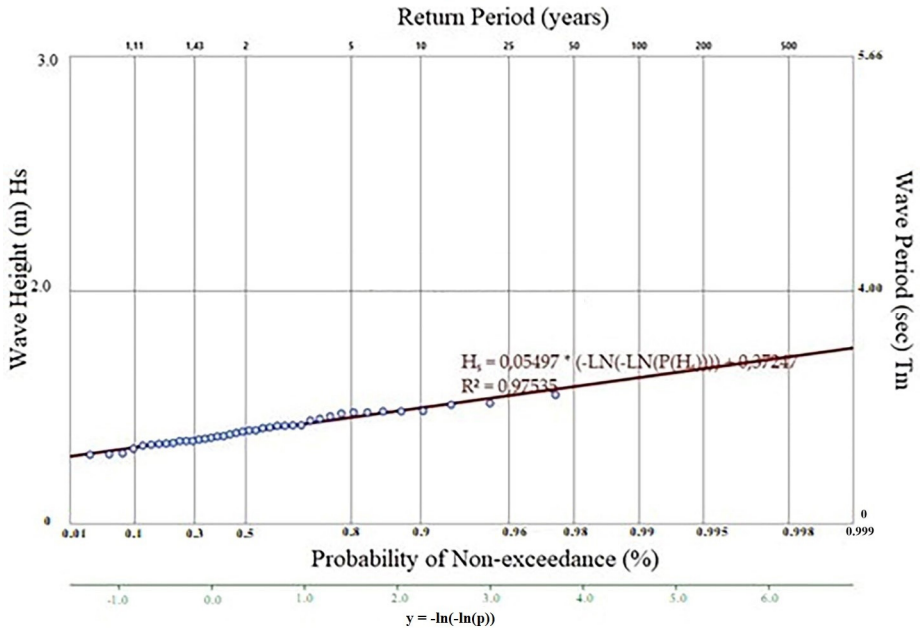

Figure 18. The Extreme Value distribution wave statistics [12].

3.4. Current Climate Sub-Model

The model uses wind forcing to simulate a continuous time series of currents in the lake, and the 3D current profile at the present MLL is displayed in Figure 19 for the construction depth of 8.50 m. The variation of the current velocity in 100 years obtained from the MCS is given in Figure 20. The circulations at Burdur Lake are irregular and turbulent in the breaking zone. The vertical isotropic k-ε model calculates the eddy viscosity values. The initial response to local force by wind stress causes the wind to set up in the lee and set down in the windward shore, creating a vertical exchange of momentum.

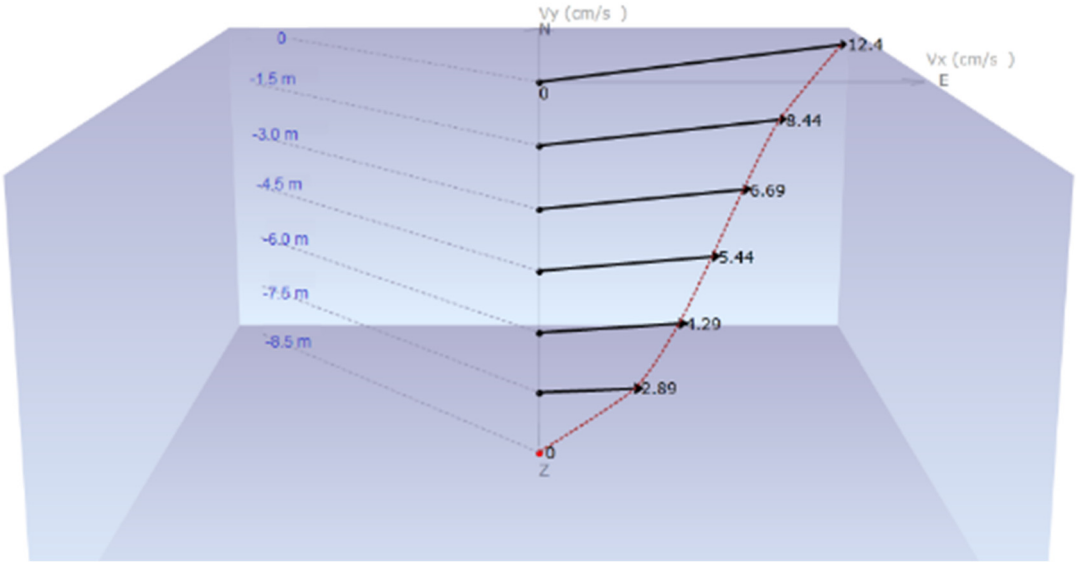

Figure 19. Three-dimensional current distribution at the design depth for a wind blowing in SW direction of 10 m/s [12].

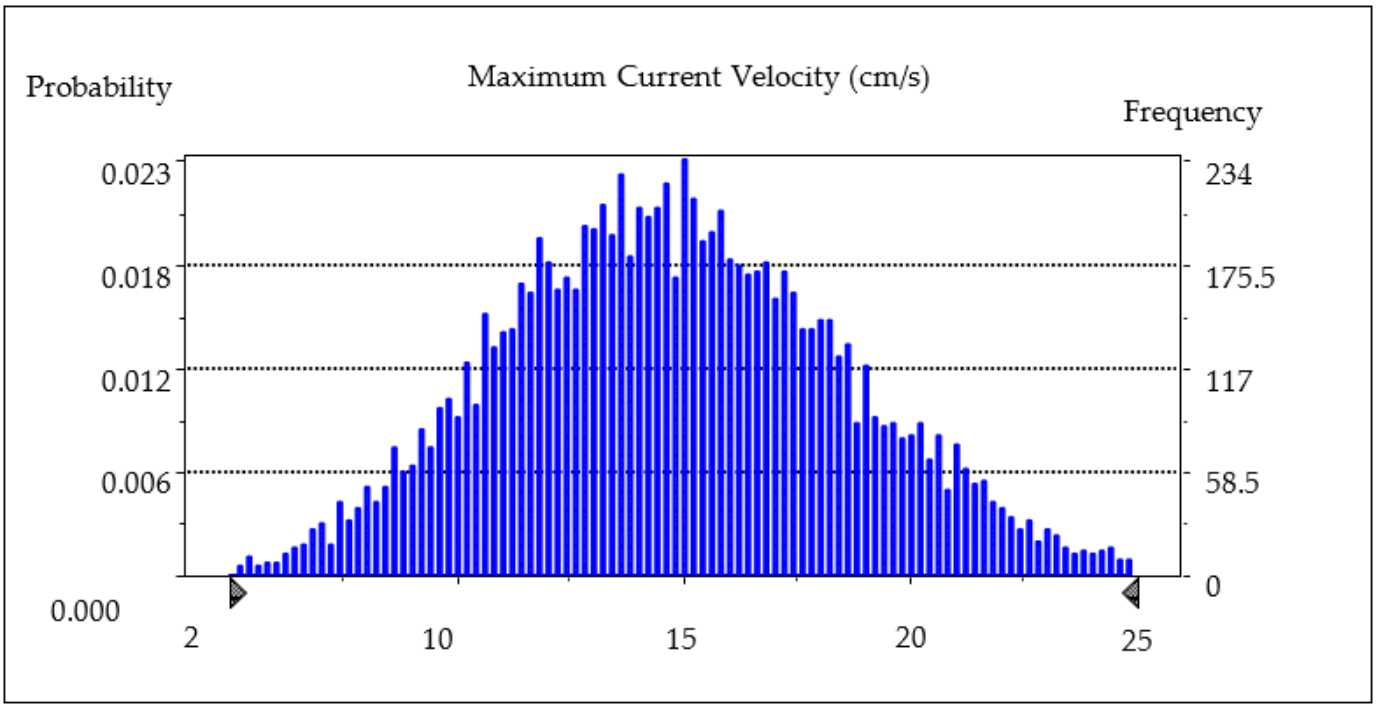

Figure 20. MCS provided the variation of maximum current velocity in the water column (cm/s) for the next 100 years.

3.5. Geotechnical Sub-Model

A systematic geotechnical investigation was carried out to define the subsurface stratigraphy and groundwater conditions, to assess the engineering characteristics of the representative soil profile, and to provide recommendations for the type, depth, and allowable bearing pressure for foundation design within the scope of the pipeline construction. For this purpose, seven cone penetration tests (CPT) with a total length of 181 m were executed (Figure 21), and seven trial pits with depths ranging from 3.0 to 3.5 m were excavated (Figure 22) in the study area. Based on field investigation and laboratory analyses of the representative soil samples, stratigraphy in the sub-surface consists of black–grey-colored

high-plasticity clay that is classified as CH according to the Unified Soil Classification System (USCS) from the surface to the maximum drilled depth of 30 m.

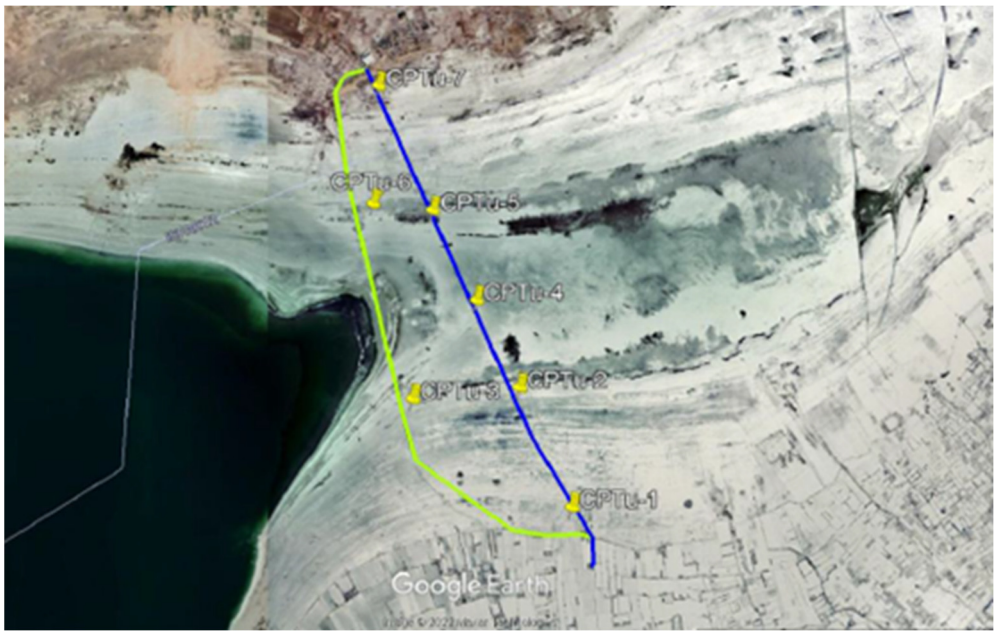

Figure 21. Location of cone penetration tests performed at the site.

Figure 22. Three of the seven exploratory trial pits were excavated at the site.

The laboratory results indicate that this clay's plasticity index (PI) changes between 35 and 40, whereas the mean natural unit weight (γ_n) is only about 15 kN/m^3. Due to the high-water content that changes between 75% and 90%, no undisturbed samples suitable for triaxial strength testing could be obtained during the field investigation.

The coefficient of the variation (COV) of the inherent variability of the total unit weight (γ) and dry unit weight (γ_d) were examined by [29]. The typical COVs for these components are smaller than 10% based on a data set comprising more than 3200 results. No trends in the COV have been detected as the mean unit weight of data varies from about 13 to 20 kN/m^3. The number of data on the scale of fluctuation is rather delimited for comparability to the number of data for the COV of inherent soil variability. From only two studies that report a vertical scale of fluctuation, an average value of 5.2 m can be chosen for the total unit weight of clay [29]. It is predicted as 1 to 2% for the COV of the

measurement error for the total unit weight and is the smallest among all the laboratory soil mechanics experiments.

To determine the total unit weight (γ_t) in the laboratory, Equation (24) turns into:

$$\xi_d = \gamma_t = e + w + t \tag{33}$$

The mean and variance of the design characteristics (γ_t) were obtained with the aid of Equation (26), displayed in the following:

$$m_{\xi,d} \approx t \tag{34}$$

$$s_{\xi,d}{}^2 \approx s_w{}^2 + s_e{}^2 \tag{35}$$

Accordingly, the COV that belongs to ξ_d, which is expressed as $s_{\xi,d}/m_{\xi,d}$, is presented as:

$$COV_{\xi,d}{}^2 \approx COV_w{}^2 + COV_e{}^2 \tag{36}$$

$COV_{\xi,d}$ is the COV of ξ_d, COV_w is the COV of the inherent variability, s_w/t, and COV_e is the COV of the measurement error, s_e/t. The COV of the spatial average (ξ_a) is similarly determined with the utilization of Equation (27):

$$COV_{\xi,a}{}^2 \approx \Gamma^2(L_a)\, COV_w{}^2 + COV_e{}^2 \tag{37}$$

in which $COV_{\xi,a}$ is the COV of ξ_a.

The COV of the inherent variability (COV_w) and measurement error (COV_e) for the dry unit weight were estimated to be a maximum of 10% and 2%, respectively. The average value for the typical vertical scale of fluctuation was determined to be 5.2 m. Using these numerical data, the total COV for the direct measurement of γ_t in the laboratory tests is 10% (Equation (31)). The depth of influence for a 1.10 m-wide pipe foundation at a depth of 2.65 was selected to be between 1.75 m and 3.50 m. Therefore, for an average dimension in length, which is 1.75 m, the amount of variance reduction [$\Gamma^2(L_a)$] will be 1.0, according to Equation (28). With the insertion of this variance reduction into Equation (32), the corresponding COV for the spatial average ($COV_{\xi,a}$) belonging to the dry unit weight would still be 10%.

For the bearing capacity calculation, the undrained shear strength (s_u) can be estimated from CPT cone tip resistance (q_t) values obtained during the field investigation. The correlation between the undrained shear strength and the corrected cone tip resistance can be expressed as in the following:

$$s_u/\sigma'_{vo} = NK(q_t - \sigma_{vo})/\sigma'_{vo} = (m_{DK} + \varepsilon)(q_t - \sigma_{vo})/\sigma'_{vo} \tag{38}$$

in which σ'_{vo} and σ_{vo} are the effective and total overburden stress, respectively, NK is the uncertain model slope, m_{DK} is the mean of NK, and ε is the zero-mean random variable representing model uncertainty [45].

Equation (34) presents the expression of the correlation model in the structure of Equation (24) as follows:

$$\xi_d = s_u = (m_{DK} + \varepsilon)(t + w + e - \sigma_{vo}) \tag{39}$$

in which $(t + w + e) = q_t$. The mean and variance for this design characteristic have been obtained from Equation (26), as shown in the following:

$$m_{\xi,d} \approx m_{NK}\,(t - \sigma_{vo}) \tag{40}$$

$$s_{\xi,d}{}^2 \approx m_{NK}{}^2\,(s_w{}^2 + s_e{}^2) + (t - \sigma_{vo})^2\, s_\varepsilon{}^2 \tag{41}$$

The COV of ξ_d has been presented by:

$$COV_{\xi,d}{}^2 \approx (COV_w{}^2 + COV_e{}^2)/(1 - \sigma_{vo}/t)^2 + COV_\varepsilon{}^2 \quad (42)$$

in which COV_ε is the COV of model uncertainty, s_ε/m_{NK}. The COV of the spatial average (ξ_a) can be similarly acquired from Equation (27):

$$COV_{\xi,a}{}^2 \approx [\Gamma^2(L_a)COV_w{}^2 + COV_e{}^2]/(1 - \sigma_{vm}/t)^2 + COV_\varepsilon{}^2 \quad (43)$$

Here, σ_{vm} is the average total overburden stress over L_a. The COVs of model uncertainty (COV_ε) were found to be between 29 and 35% by [28].

COV_ws is the COV of the inherent variability and measurement error for the cone tip resistance (q_t) in clay, which is predicted to be smaller than 20% and between 5 and 15%, respectively) [29]. The vertical scale of fluctuation for q_t in clay was less than 0.5 m. To assess Equations (36) and (37), it is also compulsory to calculate the ratios σ_{vo}/t and σ_{vm}/t. It should be indicated that t equals the mean value of q_t because the mean of w and e is zero. The field measurements show that the average value of q_t (=t) in Burdur Lake clay is around 0.5 MPa. The total overburden stress (σ_{vo} or σ_{vm}) is 45 kN/m^2 under circumstances of total soil unit weight equal to 15 kN/m^3, and the depth has an average value of 3 m. Hence, the ratios σ_{vo}/t and σ_{vm}/t are around 0.1.

Utilizing these numerical data with average values of 32% of 10% for model uncertainty and measurement error, respectively, the total COVs ($COV_{\xi,d}$) for s_u predicted from q_t would be about 40% (Equation (36)). With a mean length of 1.75 m, the measure of the variance reduction [$\Gamma^2(L_a)$] would be 0.29 according to Equation (28). With the insertion of this variance reduction into Equation (37), the corresponding COV for the spatial average ($COV_{\xi,a}$) of undrained shear strength can be obtained as 36%. The mean value of undrained shear strength becomes 28 kPa for average values of q_t = 0.5 MPa and NK = 16.

The characteristic bearing capacity of the pipe foundation for undrained conditions is given by:

$$q_c = N_c\, s_u \quad (44)$$

N_c is the bearing capacity factor equal to 7.2 for a strip foundation with a depth-to-width ratio of 2. Note that both the soil unit weight and the undrained shear strength can conveniently be characterized by a log-normal distribution, which is also predicated by the fact that they are always positive quantities [46].

3.6. MCS Sub-Model

The Morison equation is used to design pipelines concerning regulations in Türkiye [47]. The forces affecting the buried pipelines under lakes are illustrated in Figure 23 as a force balance diagram. The Morison equation is widely used in calculating hydrodynamic loads applied to cylindrical pipelines. The Morrison Equation gives reliable solutions for cases that incorporate wave–current interactions. From the 1950s, with the aid of the Morison Equation, many pipeline designs have been conducted, and only a few undesired situations have been encountered. As a result, the Morison Equation has provided reliability in the design of pipes for over half a century [48]. The design of submarine pipeline systems necessitates considering various hydrodynamic loads following the Det Norske Veritas (DNV) standard ST-F101 [49].

Specifically, this standard emphasizes the importance of considering the lift force subject to variations due to the wave action. The 3-D hydrodynamic model must be employed to comply with the requirements set forth by the DNV standard, as the applied wave theory in the model accurately characterizes wave kinematics at the construction depth of the pipes, including the surf zone hydrodynamics.

Moreover, to consider the influence of currents on submarine pipelines, the drag and lift forces are combined with the wave-induced forces by applying theories for

wave–current interactions. Thus, developing a hybrid model that integrates wave and current forces is fundamental to fulfilling the constraints of standards.

Figure 23. Force balance diagram of the pipeline installed in the trench.

As a result, the actions of lift force (F_L) and the combined wave and current are simulated in the MCS sub-model using the conclusions of the 3D hydrodynamic model. Since the pipeline will be buried, the vertical limit state function is considered for the preliminary design, as illustrated in Figure 24. Although the pipe is buried, waves can affect the pipes due to the permeable structure of the sub-base.

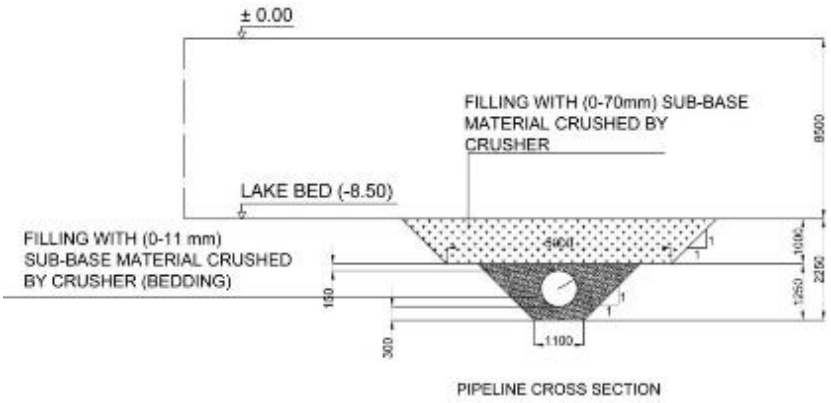

Figure 24. Preliminary design for the pipeline trench in Burdur Lake.

Here, the lift (F_L) and the resultant contact (F_C) forces can be expressed as given in Equations (45) and (46):

$$F_L = \frac{1}{2}\rho_w D C_M \left(V_s\, cos\Theta + V_c\right)^2 \tag{45}$$

$$F_C = W_S + W_f + W_c \tag{46}$$

where W_c is the weight of the water, F_c is the contact force of the soil, D is the pipeline diameter, W_S is the submerged pipe weight, W_f is the saturated fill weight, V_C is the lake current velocity, Θ is the phase difference, and C_M is the inertia coefficient. The first-order wave bottom velocity (V_S) is:

$$V_s = \frac{\pi H}{T} \cdot \frac{1}{\sinh\left(\frac{2\pi d}{L}\right)} \tag{47}$$

where H is the wave height, d is the depth, and T and L are the wave period and wavelength, respectively. The first limit state function of pipe stability in the vertical direction is given by Equation (48):

$$Z_{V1} = (Fc - FL)/\gamma_{sc} > 1 \quad (48)$$

where γ_{SC} is expressed as the partial safety factor.

The balance between the pipe contact force and the bearing capacity of the soil beneath it determines the embedment depth of the pipe. DNV-GL-RP-[50], a recommended practice by Det Norske Veritas (DNV), outlines the limit state function of the embedment, which occurs when subjected to undrained loading conditions. Specifically, the second limit state function that should be satisfied, as given by the DNV standard ST-F101 for pipeline stability [49], is defined in Equation (49) as the exceedance of the bearing capacity of the soil:

$$Z_{v2} = \frac{\frac{q_c}{\gamma_{Rv}}}{F_C} \geq 1.0 \quad (49)$$

in which γ_{Rv} is the partial safety factor for the bearing capacity defined as 1.4 in Turkish Earthquake Resistant Building Code [51].

All the random variables in the limit state functions are modeled by probability distributions in the MCS, as defined in Table 1, and their randomly generated samples are created for 30,000 simulations as illustrated in Figures 25 and 26.

Table 1. The probability distributions used in MCS.

Parameters	Description	Minimum	Average	Maximum	Standard Deviation	Type	Distribution
Z_{V1}	Vertical limit state	1.04	3.21	4.23	0.14	Simulated (Figure 25)	
Z_{v2}	Bearing capacity of soil	1.05	3.26	7.82	0.22	Simulated (Figure 26)	
C_M	Inertia coefficient	1.10	2.00	2.90	0.30	Normal	
γ_{sc}	Safety factor	1	2	3	0.50	Triangle	
V_c	Bottom Current (m/s)	0.03	0.15	0.26	0.05	Simulated (Figure 20)	
V_s	Bottom velocity of wave (m/s)	0.05	0.20	0.35	0.05	Log-normal	
ρ_w	Fluid density (N/m^3)	970	1000	1030	10	Log-normal	
γ_t	Soil unit weight (kN/m^3)	13	15	16	1.5	Log-normal	
Wf	Weight of filling material (kg)	1440	1600	1760	10	Triangle	
ds	Construction depth (m)	7.90	8.00	8.10	0.05	Simulated (Figure 11)	

Table 1. *Cont.*

Parameters	Description	Minimum	Average	Maximum	Standard Deviation	Type	Distribution
Wc	Weight of water column (kg)	720	800	880	10	Triangle	
s_u	Undrained shear strength (kPa)	10	28	50	10.08	Log-normal	
W_{block}	Concrete fixation blocks (t/m)	0.30	0.52	0.90	0.10	Log-normal	
$W_{friction}$	Piles (t/m)	15	20.75	27	2	Log-normal	

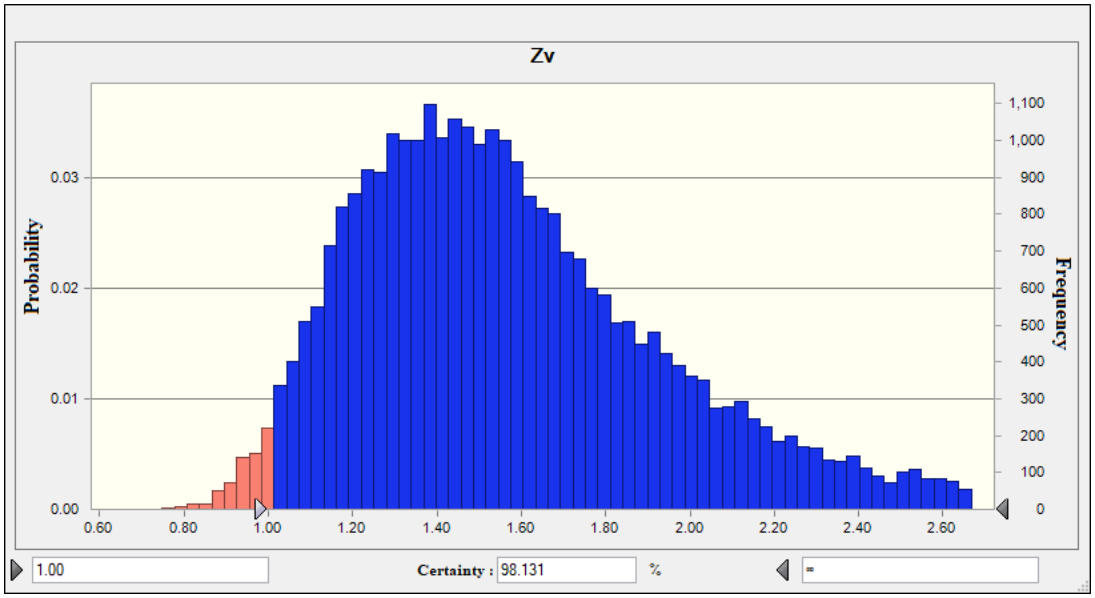

Figure 25. The pipe failure's vertical limit state function (ZV_1) in its lifetime for D = 0.8 m.

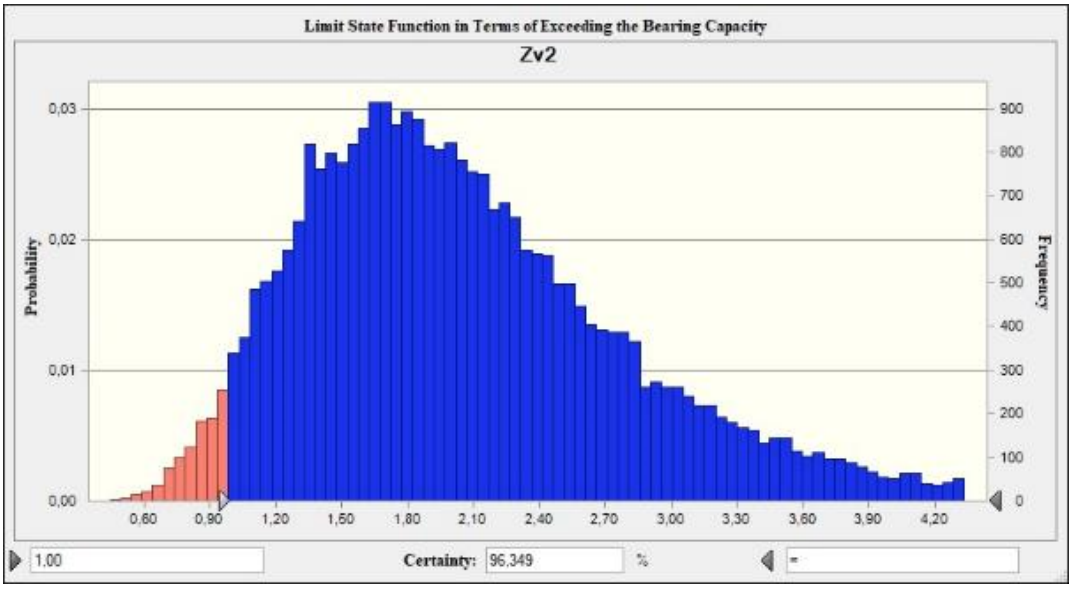

Figure 26. The second limit state function (Z_{V2}) exceeds the bearing capacity.

4. Design in the Imminent Climate Change Era

Considering all the uncertainties in design in the global warming era is crucial. Primarily, the pipeline is considered without pile foundations in the deterministic design. It can be seen from Figures 25 and 26 that the structure will not protect its integrity under the computed conditions, with an average failure probability of 1.86% and 3.65%. Followingly, the pipeline is computed as a piled system under the pipeline. This condition gives the desired results for the design procedure. The failure probability is around 0.05% for this design condition. The MCS conducts all the design procedures for both design conditions. A deterministic design does not possess the ability to compute accurate design failure probabilities. Hence, the MCS provides a precious sight for engineers. The MCS computes 30,000 different scenarios, and each one is also a real situation. In this respect, the MCS differs from a deterministic design.

4.1. Vertical Stability of Preliminary Design

The result of the MCS for the vertical limit state function (Z_{V1}) of the pipe failure in its lifetime of 50 years for a design diameter of D = 0.8 m was depicted in Figure 25. The figure indicates that the lifetime failure probability of the pipeline is approximately 3.4% when considering environmental risk parameters such as climate change, storms, lake level changes, and the breaking of waves. In this figure blue zone designates the reliability and red zone indicates failure.

Integrating future changes in environmental conditions increases the risk of pipeline failure, which is unacceptable according to the DNV ST-F101 standard for pipeline stability [50]. After the simulations, the most important design parameters were identified through a sensitivity analysis, as shown in Figure 27, for a pipeline diameter of 0.8 m. The sensitivity analysis illustrated the contribution of the variability of each random design variable in the MCS. Figure 27 shows the sensitivity analysis with the contribution of different pipeline variables. The MCS, which is applied to the limit state, integrates the cumulative effect of various design components and the comparative analysis of the effect ratio of every component.

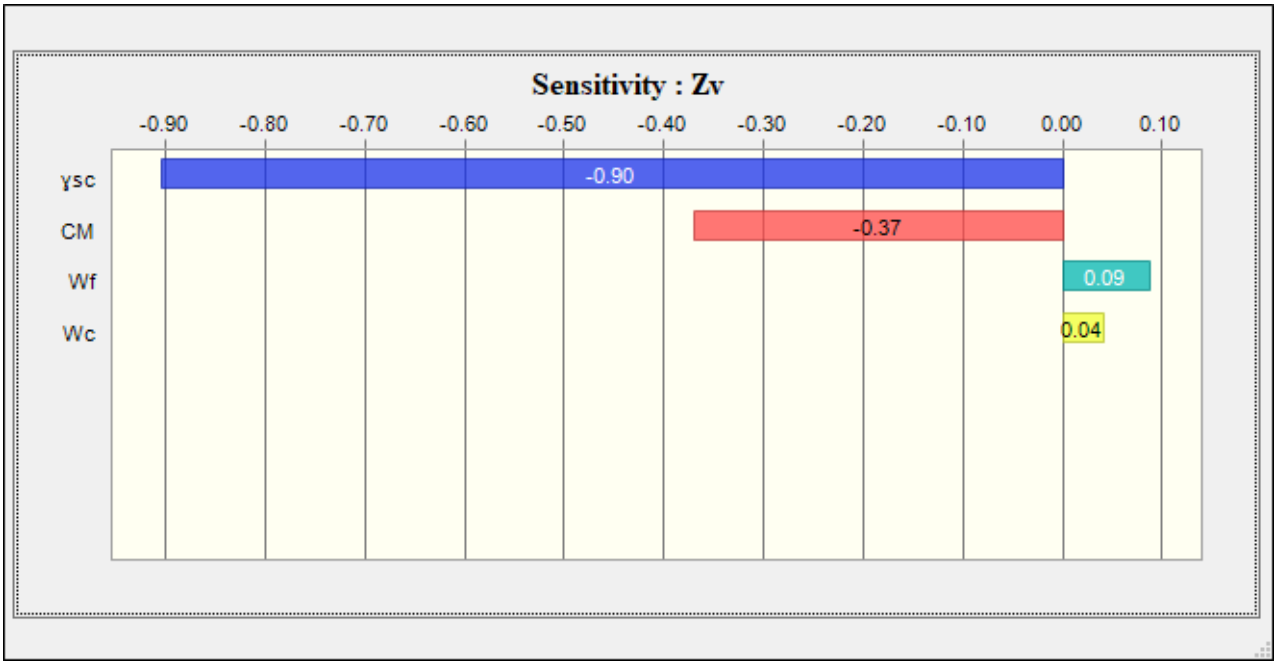

Figure 27. The sensitivity chart of design variables for Z_{v1}.

The correlation of the design variables is presented in terms of scatter diagrams in Figure 28. It can be used to discover if the stability of the pipeline is positively or negatively

correlated with certain design variables. The safety factor (γ_{sc}) affects the limit state function with a correlation of $\rho = -0.9721$, indicating that as the factor decreases, the limit state function is inversely affected. The coefficient of inertia (C_M) of the pipe also negatively affects the limit state function, with a much smaller correlation of $\rho = -0.152$ compared to γ_{sc}, highlighting the relative importance of pipe characteristics. Thus, although at a smaller scale, the geometric and material characteristics of the pipe also influence the limit state.

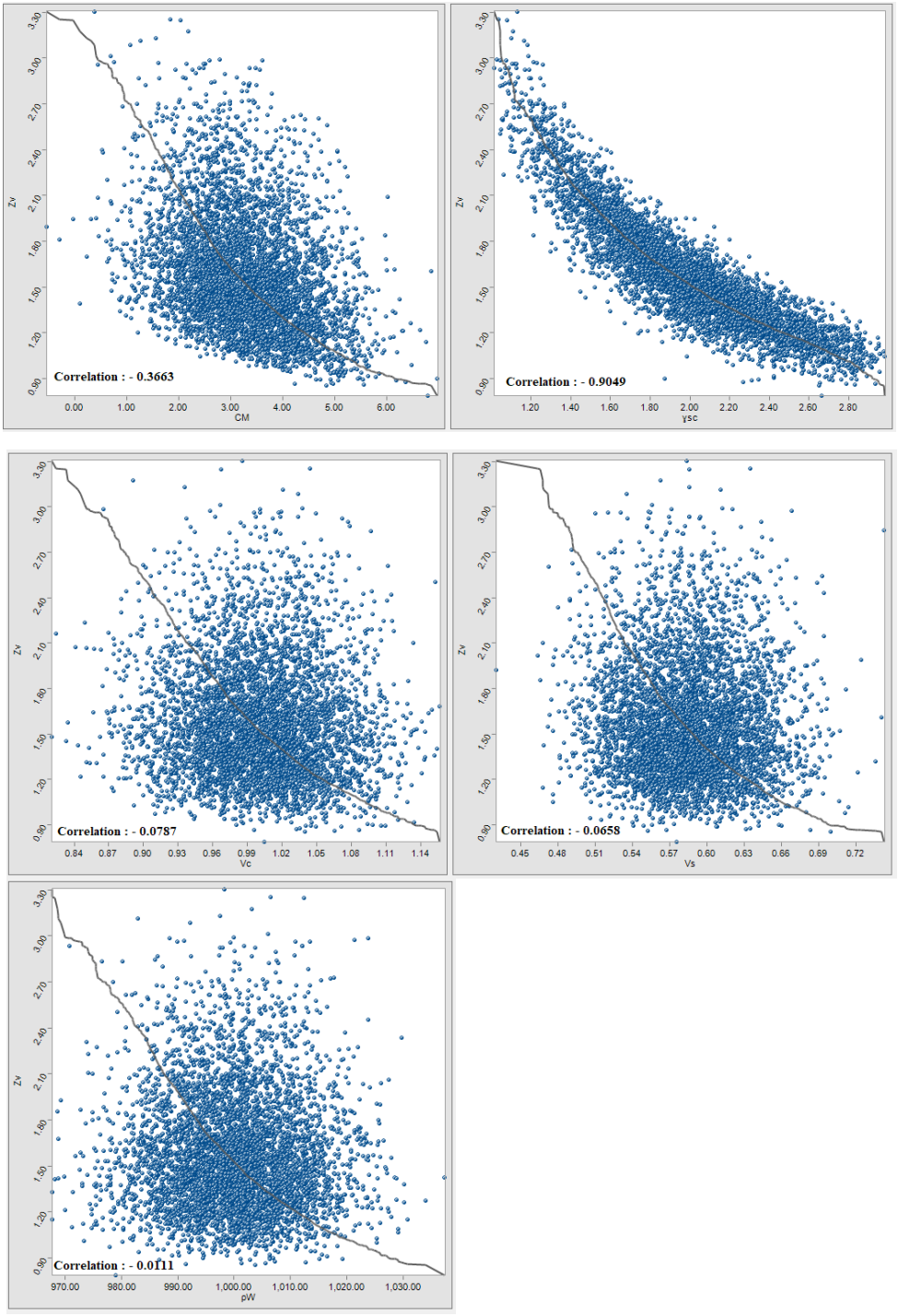

Figure 28. Scatter diagrams of the correlation of design variables for Z_{v1}.

The current velocity (V_c) negatively correlates with stability, with a correlation of $\rho = -0.088$, suggesting the stability is still slightly impacted by currents despite the buried pipeline emphasizing the significance of wave breaking. Furthermore, the bottom wave

velocity (V_s) negatively affects stability, with a correlation of $\rho = -0.084$, indicating that the wave amplitude also, although only slightly, affects the pipe. Hence, waves can influence stability up to a certain soil depth due to the permeable sub-base material. The fluid density (ρ_w) transported in the pipe negatively affects stability, with a correlation of $\rho = -0.026$, signifying that if the transported fluid is lighter than water, it has a small negative correlation as it contributes to buoyancy.

4.2. Bearing Capacity of Preliminary Design

The second limit state function should satisfy the DNV standard ST-F101 [49], as defined in Equation (49) for the exceedance of the bearing capacity of the soil. The safety of the design is obtained by considering the burial depth for the bearing capacity of the soil. From the MCS of the second limit state function, Z_{v2}, the failure probability of the pipe is determined to be 3.65%, as illustrated in Figure 26, which does not satisfy the related DNV standard ST-F101 for pipeline stability [49], as the target failure probabilities per pipeline should be in the order of 10^{-2} for a low safety class [50]. In Figure 26, blue zone designates the reliability and red zone indicates failure.

Figure 29 presents the sensitivity chart of design variables for bearing capacity. From the sensitivity study of design variables for the bearing capacity, the variation in undrained shear strength (s_u) exhibits a direct effect (99.9%) on the bearing capacity. Certainly, the undrained shear strength (s_u) is the most significant parameter affecting the simulation results, given its stated variability. On the other hand, the saturated weight of the fill material (W_f) and the weight of the water column (W_c) negatively affect the soil-bearing capacity at a 10^{-2} significance level in the MCS.

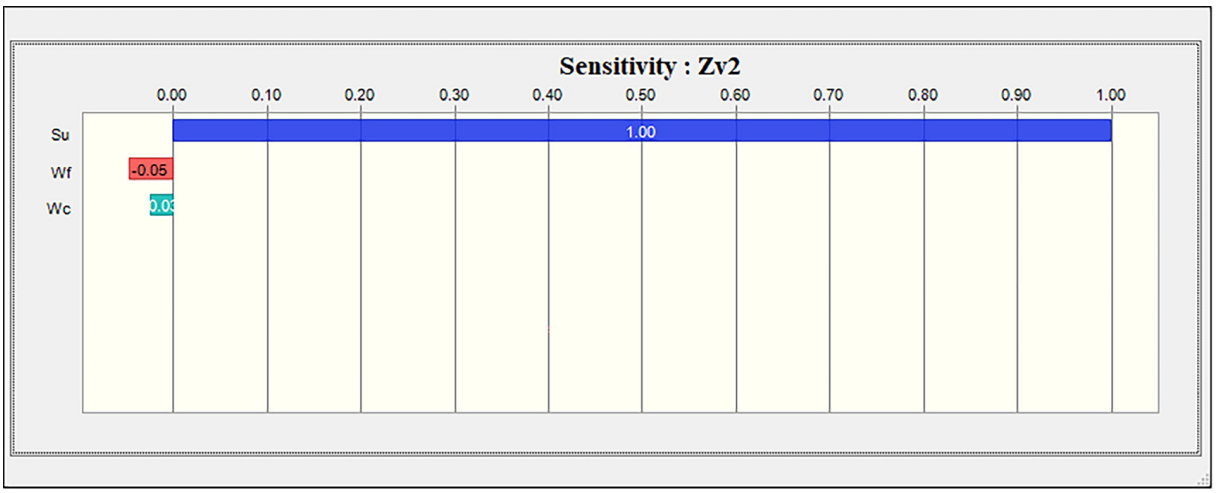

Figure 29. The sensitivity chart of design variables for bearing capacity.

As a result, the lifetime failure probability of the pipeline for vertical stability is approximately 3.65% when considering both limit states and all the environmental risk parameters such as climate change, storms, lake level changes, and the breaking of waves. Therefore, the preliminary design was not verified for the vertical limit state, considering the inherent variations due to lake level changes and climate change. However, if such a hybrid model had not been developed and environmental parameter variations had not been considered, the deterministic design could have been approved by the existing design code in Türkiye, demonstrating the importance of a hybrid model in fulfilling standards and ensuring a safe design when considering the city's drinking water project's status.

4.3. Vertical Stability of Final Design

The results obtained from the hybrid model have revealed that pipeline stability has a higher failure probability than the acceptable risk given by the DNV standards when exposed to the combined influence of waves and currents.

To mitigate the buoyancy forces arising from the underground water level and to achieve the nominal target failure probability, which is on the order of 10^{-2} for the limit state, the design was altered by the installation of concrete fixation masses every six meters along the pipeline, as well as the incorporation of 7 m-long 60 cm-diameter concrete tension piles, as depicted in Figure 30.

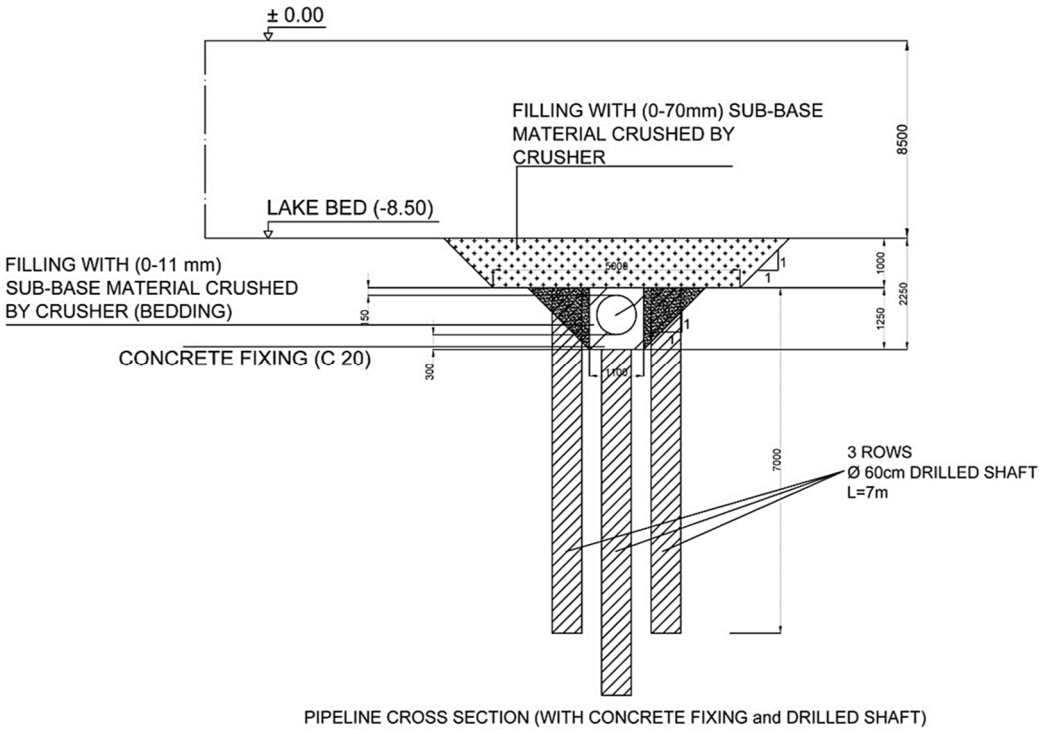

Figure 30. The final design will use concrete fixing and supporting piles.

The outcome of this modification is a revised contact force (Fc) as outlined in Equation (50):

$$F_C = W_S + W_f + W_c + W_{block} + W_{pile} \tag{50}$$

where W_f is the skin friction force around the piles, W_{block} and W_{pile} are the weight of the concrete fixation blocks and piles, respectively. These counter forces are considered per meter of the pipeline in the MCS. W_f is given in Equation (51):

$$Wf = \alpha * s_u * p * L \tag{51}$$

where α = 0.55 for s_u < 150 kPa; p is the perimeter of the pile (m), and L is the length of the pile (m).

When the concrete fixation masses and tension piles are added to the design, the lifetime exceedance probability of the vertical limit state decreases to 0.32%, signifying the increased capacity of vertical stability concerning the uncertainty of hydrodynamic loads, as illustrated in Figure 31. In this figure blue zone designates the reliability and red zone indicates failure. Now, the modified design satisfies the DNV ST-F101 standard for pipeline stability [50], integrating future changes in environmental conditions in the hybrid model. The target failure probabilities per pipeline should be 10^{-2} for a low safety class [50].

Integrating concrete masses and tension piles into the pipeline system's design significantly reduced its lifetime failure probability. Specifically, the modifications led to the pipeline system meeting the nominal target failure probability, and the failure probability was obtained from the MCS as 5.3×10^{-2}, which follows the serviceability limit state prescribed by the DNV standard. As a result, the modified design with concrete fixation masses and tension piles presented in Figure 31 satisfies the target lifetime failure probability when both the pipe–soil interaction and vertical stability are concerned.

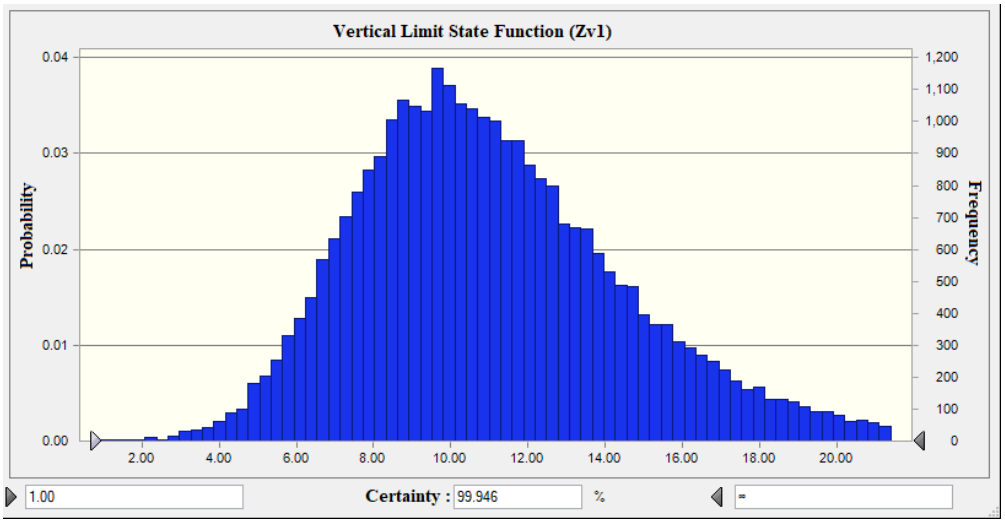

Figure 31. The pipe failure's vertical limit state function (ZV_1) in its lifetime for D = 0.8 m for the new design with concrete fixation masses and tension piles.

4.4. Bearing Capacity of Final Design

The second limit state function should satisfy the DNV standard ST-F101 [49] as defined in Equation (49) for the exceedance of the bearing capacity of the soil. The safety of the modified design is obtained by considering the pipe's embedment depth for the soil's bearing capacity. From the MCS of the second limit state function, Z_{v2}, the failure probability of the pipe due to bearing capacity failure, is determined to be 5.3×10^{-2}, as illustrated in Figure 32, which satisfies the DNV standard ST-F101 for pipeline stability [49], as the target failure probabilities per pipeline should be in the order of 10^{-2} for a low safety class [50]. In Figure 32, blue zone designates the reliability and red zone indicates failure.

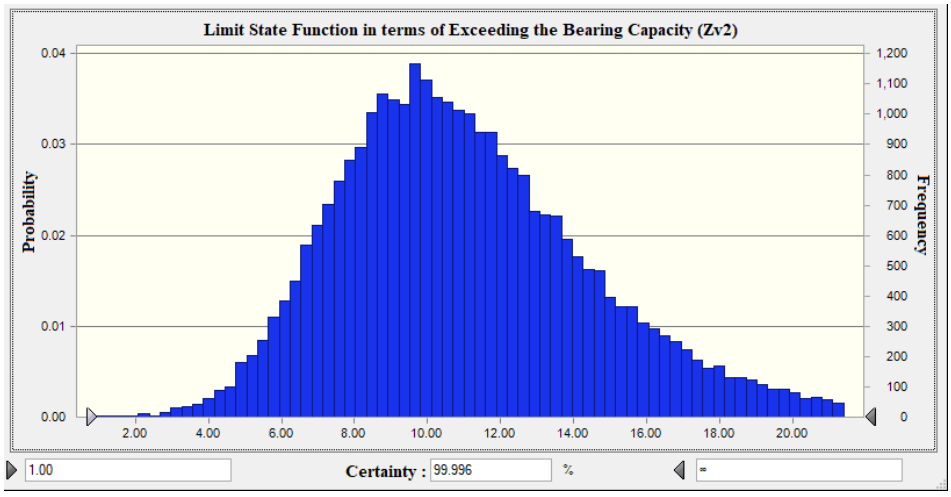

Figure 32. The second limit state function (Z_{V2}) of the bearing capacity for the final design.

The presented model was developed to address the limitations of existing design methods by ensuring comprehensive environmental considerations and enhancing reliability through advanced simulation techniques. The first part of the design, which includes bearing studies without piles, demonstrates a significantly higher failure probability than the final design, which incorporates concrete fixation masses and tension piles.

These two stages of design are vastly different from each other. With its higher failure probability, the initial design underscores the importance of pile construction for achieving stability and compliance with standards. The final design mitigates buoyancy forces and

achieves the nominal target failure probability, thus satisfying the DNV ST-F101 standard for pipeline stability by integrating future environmental changes into the hybrid model.

As a result, the first part of the design contains bearing studies without piles. However, the final part is crucial, while the first part has a considerably high probability of failure without pile construction; they are vastly different from each other.

5. Discussion of the Results

This study aimed to evaluate the limit-state probabilities and consequences related to pipeline failure through an extensive risk assessment approach. The statistical Monte Carlo Risk Sub-model developed for pipeline design was used to examine the pipe's stability for risk analysis. This study's hybrid MCS model provided a reliable technique for predicting pipeline stability. The proposed hybrid risk assessment model is based on analyzing factors that contribute to the overall risk of a submarine pipeline, such as environmental conditions, the geotechnical integrity of the pipeline, and any external sources of risk.

The methodology begins by determining the wind, wave, and current climates and climate change effect. A case study was conducted to illustrate the confidence level of the methodology. A pipeline project constructed on the lakebed to provide drinking water to the province of Burdur, which had lost its operational capability, was considered. The surface area of Burdur Lake has decreased dramatically in the last decade, and the pipeline has become visible on the lakebed. Under this circumstance, the pipeline system has become vastly open to meteorological effects such as wind, flood, and storms. The system became vulnerable to all environmental conditions. The surface area of Burdur Lake experienced a 40% decline from 1986 to 2019 due to a 30% decrease in the total precipitation. The MCS approach was employed to assess the effects of climate change and the decrease in the surface area of the lake on the pipeline, in conjunction with the Hydrotam 3D model, to simulate the variation in the Mean Lake Level (MLL) and determine the variation in the depth of construction for the pipeline system.

This approach revealed that the MLL would decrease by 53 cm over the next 100 years at the construction depth of the pipeline, and climate change scenarios were incorporated into the water level analysis for the pipeline design.

The wind statistics of the region were analyzed using ECMWF ERA5 and operational archive 6-h wind forecasts, identifying a fetch distance of 20 km in the West–West Southwest (W-WSW) direction segment. In the worst-case scenario, the maximum significant wave height for the pipeline design was determined as Hs = 1.2 m.

Such considerations shall allow designers to design more adaptable pipelines suitable for withstanding the changing conditions of global warming. In the pipeline system, a hybrid MCS-based approach confirms user reliability and design safety. This method considers a range of uncertainties and risks that can affect the functioning of the pipeline and ensures that the required safety standard is reached. With the MCS approach and coupling of the Hydrotam 3D model, it will be possible to simulate the variation in MLL to see its variation in the depth of construction for the pipeline system. Moreover, it has been decided to study the statistical data of the area's wind and wave climate to ensure that, while the pipeline is designed, dynamic conditions are also evoked by storm surges. It also considers the soil parameters variable, considering the design's probability of bearing capacity failure. These considerations will allow pipeline designers to develop sturdier structures against the changing conditions that prevail from global warming.

The proposed methodology would be capable of identifying the areas that would benefit from the risk mitigation of some of the risks due to the operation of the submarine pipeline, ultimately allowing them to lower the risk of damage due to environmental conditions. Most of these installations, especially in the beds of the lakes and other bodies of water, will call for thorough considerations of global warming and changing climatic conditions. By coupling the MCS approach with the 3D Hydrotam model, a proper methodology for predicting the variations in the mean lake level (MLL) and ascertaining the proper depth of the pipeline system is devised. For this, the wave climate study of the region

and wind statistics were also performed to ensure that the designed pipeline can resist the dynamic conditions emanating from storm surges and floods.

This case would put the pipeline designers in a better position to consider these factors for developing more sustainable and resilient structures to understand the changing environmental conditions emanating from global warming. Hence, the hybrid model can evaluate the reliability of the pipelines, considering environmental and climate parameters. The Hydrotam 3D model was used to obtain the variations in these parameters and their influence on the stability. Hence, the model is used during the pipeline's design process to decrease the risks that could arise from the pipeline's operation and guarantee stability and reliability.

6. Conclusions

The Hybrid 3D Hydrodynamic MCS (HMCS) Model is presented for the risk assessment and design of marine structures under the influence of global warming and climate change. The model can improve the resilience and sustainability of maritime infrastructures against environmental uncertainties by incorporating the risk-based approach. The HMCS model can efficiently simulate the interaction of marine structures with environmental parameters—such as wind, waves, storms, and geotechnical conditions—permitting enhanced design strategies that are more resilient to climate-induced vulnerabilities. As climate change continues to impose risks to infrastructure, implementing such advanced, risk-based design models is necessary to guarantee maritime structures' long-term safety and functionality. The outcomes encourage modifying existing design codes to include the hybrid model so maritime structures can endure the evolving challenges of climate change.

The hybrid model is systematically efficient and assesses the impacts of global warming with changing climatic conditions on pipeline systems so that more resilient and sustainable infrastructure can be developed. Therefore, providing a risk-based design approach for maritime structures, such as submarine pipelines, ensures long-term safety and serviceability. The uncertainties and risks from climatic change can be considered in the design, so the maritime structure will be constructed to be resilient to it.

The HMCS model is a very powerful tool for the risk assessment of maritime structures because it includes sub-models, considering all major environmental factors that could affect the stability of the structure. Hence, the model will be useful in simulating the structural behavior under environmental conditions. Such results may be used in designing maritime structures that are more resistant to the vulnerability created by climate change. Climate change has been an issue of concern for the last few decades since many devastating impacts have been observed in various sectors of life, including the design and reliability of infrastructures.

This study sheds light on the effect climate change and water level variations might have on lake and marine structures, using the example of a pipeline crossing through a lake. The pipeline through the lake is highly exposed to breaking wave effects, damage, breakage, and malfunction concerning the dwindled levels of water that might have been because of climate change. It is, therefore, exposed in the drying part of the lake, clearly showing the future impacts of climate change. It is, therefore, crucial to develop design methods that consider the effect and risk caused by the climate in the design of the structure related to the sea and lakes.

Current deterministic design methods may not address the impact of climate change on marine and coastal structures. The lack of water level predictions caused by climate change can damage, break, and, in any case, cause a malfunction of the pipeline. Hence, the pipeline is exposed in the drying part of the lake, showing very clearly the warning signs towards the ensuing impacts of climate change in the next few years. Therefore, there is a vital need for design methodologies that consider the effects and risks of climate change in designing these maritime structures.

New standards and regulations for designing marine and coastal structures must be developed to consider the effects of climate change using this model. This paper attempts to

present a design approach that encompasses a risk-based philosophy to cover the limitations of the current deterministic design methods and codes. The developed hybrid model for the pipeline brings out the fragility of the structure to environmental future effects, which is not normally captured through standard design methods. Hence, redrafting current design codes is necessary, and subsequently, risk-based practice is needed to ensure structures exhibit credibility and reliability in the changing climate. If such innovative design methods are not implemented, structures designed using deterministic methods may lose their safety and serviceability in the climate change era. Therefore, adopting such a risk-based design model is crucial to ensure infrastructure sustainability in the face of climate change.

Author Contributions: Conceptualization, E.A.B.; Methodology, C.E.B. and S.O.A.; Software, C.E.B.; Formal analysis, A.U.; Data curation, A.U.; Writing—original draft, C.E.B.; Visualization, E.A.B. All authors have read and agreed to the published version of the manuscript.

Funding: This research received no external funding.

Institutional Review Board Statement: Not applicable.

Informed Consent Statement: Not applicable.

Data Availability Statement: Data are contained within the article.

Acknowledgments: The authors thank the HYDROTAM-3D Version 0.28 and DLTM Software Technologies in the Gazi University Technopark.

Conflicts of Interest: The authors declare no conflict of interest.

References

1. Li, X.; Chen, G.; Zhu, H.; Zhang, R. Quantitative risk assessment of submarine pipeline instability. *J. Loss Prev. Process Ind.* **2017**, *45*, 108–115. [CrossRef]
2. Chen, R.; Wu, L.; Zhu, B.; Kong, D. Numerical modelling of pipe-soil interaction for marine pipelines in sandy seabed subjected to wave loadings. *Appl. Ocean. Res.* **2019**, *88*, 233–245. [CrossRef]
3. Durap, A.; Balas, C.E.; Çokgör, Ş.; Balas, E.A. An Integrated Bayesian Risk Model for Coastal Flow Slides Using 3-D Hydrodynamic Transport and Monte Carlo Simulation. *J. Mar. Sci. Eng.* **2023**, *11*, 943. [CrossRef]
4. Barrette, P. Offshore pipeline protection against seabed gouging by ice: An overview. *Cold Reg. Sci. Technol.* **2011**, *69*, 3–20. [CrossRef]
5. Chakraborty, D. Probabilistic Uplift Resistance of Pipe Buried in Spatially Random Cohesionless Soil. *Proc. Natl. Acad. Sci. India Sect. A Phys. Sci.* **2023**, *93*, 355–368. [CrossRef]
6. Liu, P.; Meijer, A.; DeGeer, D.; Jurdik, E.; Chaudhuri, J.; Zhou, S. Probabilistic Wall Thickness Verification for the TurkStream Pipeline. In Proceedings of the ASME 2018 37th International Conference on Ocean, Offshore and Arctic Engineering, Madrid, Spain, 17–22 June 2018. [CrossRef]
7. Bhardwaj, U.; Teixeira, A.P.; Guedes Soares, C. Uncertainty in the Estimation of Partial Safety Factors for Different Steel-Grade Corroded Pipelines. *J. Mar. Sci. Eng.* **2023**, *11*, 177. [CrossRef]
8. Lin, X.; Shao, G. Application of HMC-SS Method in Pipeline Reliability Analysis and Residual Life Assessment. *Math. Probl. Eng.* **2021**, *2021*, 3756441. [CrossRef]
9. Bruce, L.C.; Frassl, M.A.; Arhonditsis, G.B.; Gal, G.; Hamilton, D.P.; Hanson, P.C.; Hetherington, A.L.; Melack, J.M.; Read, J.S.; Rinke, K.; et al. A multi-lake comparative analysis of the General Lake Model (GLM): Stress-testing across a global observatory network. *Environ. Model. Softw.* **2018**, *102*, 274–291. [CrossRef]
10. Yakar, M.; Yıldız, F.; Metin, A.; Uray, F.; Ulvi, A.; Karasaka, L.; Mutluoglu, O.; Seker, D.Z. Photogrammetric Measurement of The Meke Lake and Its Environment with Kite Photographs to Monitoring of Water Level to Climate Change. In Proceedings of the ISPRS Commission V Mid-Term Symposium, International Archives of the Photogrammetry, Remote Sensing and Spatial Information Sciences, Newcastle upon Tyne, UK, 21–24 June 2010; Volume XXXVIII, Part 5. pp. 613–615.
11. Dong, J.; Asif, Z.; Shi, Y.; Zhu, Y.; Chen, Z. Climate Change Impacts on Coastal and Offshore Petroleum Infrastructure and the Associated Oil Spill Risk: A Review. *J. Mar. Sci. Eng.* **2022**, *10*, 849. [CrossRef]
12. HYDROTAM-3D. HYDROTAM-3D, Three Dimensional Hydrodynamic Transport and Water Quality Model (6.3). 2023. Available online: http://www.hydrotam.com/ (accessed on 14 April 2024).
13. Balas, E.A. A hybrid Monte Carlo simulation risk model for oil exploration projects. *Mar. Pollut. Bull.* **2023**, *194*, 115270. [CrossRef]
14. Balas, L. Modelling of Interaction between Surface Waves and Mud Layer. In *Computational Science—ICCS 2004*; Springer: Berlin/Heidelberg, Germany, 2004; pp. 618–621. [CrossRef]
15. Balas, L.; Genc, A.N.; Eser, E. Transitional Waters Typology in Turkey: Melen Estuary Case Study. *J. Coast. Res.* **2020**, *95*, 18–22. [CrossRef]

16. Balas, L.; Inan, A.; Genc, A. Modelling of Dilution of Thermal Discharges in Enclosed Coastal Waters. *Res. J. Chem. Environ.* **2013**, *17*, 82–89.
17. Balas, L.; Inan, A.; Yılmaz, E. Modelling of sediment transport of Akyaka Beach. *J. Coast. Res.* **2011**, *64*, 460–463. Available online: http://www.jstor.org/stable/26482214 (accessed on 14 April 2024).
18. Balas, L.; Kücükosmanoglu, A. 3-D Numerical Modelling of Transport Processes in Bay of Fethiye, Turkey. *J. Coast. Res.* **2006**, *3*, 1529–1532. Available online: http://www.jstor.org/stable/25743011 (accessed on 14 April 2024).
19. Balas, L.; Özhan, E. An implicit three-dimensional numerical model to simulate transport processes in coastal water bodies. *Int. J. Numer. Methods Fluids* **2000**, *34*, 307–339. [CrossRef]
20. Balas, L.; Özhan, E. Applications of a 3-D Numerical Model to Circulation in Coastal Waters. *Coast. Eng. J.* **2001**, *43*, 99–120. [CrossRef]
21. Balas, L.; Özhan, E. Three-dimensional Modelling of Stratified Coastal Waters. *Estuar. Coast. Shelf Sci.* **2002**, *54*, 75–87. [CrossRef]
22. Balas, L.; Özhan, E. A Baroclinic Three Dimensional Numerical Model Applied to Coastal Lagoons. In *Computational Science—ICCS 2003*; Springer: Berlin/Heidelberg, Germany, 2003; pp. 205–212. [CrossRef]
23. Copernicus Climate Change Service (C3S); ERA5: Fifth Generation of ECMWF Atmospheric Reanalyses of the Global Climate, Copernicus Climate Change Service Climate Data Store (CDS), Reading, UK. Available online: https://cds.climate.copernicus.eu/cdsapp#!/home (accessed on 14 April 2024).
24. Harris, I.; Osborn, T.J.; Jones, P.; Lister, D. Version 4 of the CRU TS monthly high-resolution gridded multivariate climate dataset. *Sci. Data* **2020**, *7*, 109. [CrossRef]
25. Ebersole, B.A. Refraction-Diffraction Model for Linear Water Waves. *J. Waterw. Port Coast. Ocean. Eng.* **1985**, *111*, 939–953. [CrossRef]
26. Balas, L.; Inan, A. A Numerical Model of Wave Propagation on Mild Slopes. *J. Coast. Res.* **2002**, *36*, 16–21. [CrossRef]
27. Goda, Y. Reanalysis of Regular and Random Breaking Wave Statistics. *Coast. Eng. J.* **2010**, *52*, 71–106. [CrossRef]
28. Kulhawy, F. On Evaluation of Static Soil Properties. In *Stability and Performance of Slopes and Embankments II*; American Society of Civil Engineers: Reston, VA, USA, 1992; pp. 95–115.
29. Phoon, K.-K.; Kulhawy, F.H. Characterization of geotechnical variability. *Can. Geotech. J.* **1999**, *36*, 612–624. [CrossRef]
30. Filippas, O.B.; Kulhawy, F.H.; Grigoriu, M.D. Reliability-Based Foundation Design for Transmission Line Structures. Osti.Gov, EPRI-EL-5507-Vol.3. 1988. Available online: https://www.osti.gov/biblio/5943934 (accessed on 14 April 2024).
31. Benjamin, J.R.; Cornell, C.A. *Probability, Statistics and Decision for Civil Engineers*; McGraw-Hill: New York, NY, USA, 1970.
32. Vanmarcke, E. *Random Fields: Analysis and Synthesis*; The MIT Press: Cambridge, MA, USA, 1983.
33. Burdur Governorship. VALİ ARSLANTAŞ'TAN SENİR-BURDUR İÇME SUYU PROJESİNE YAKIN TAKİP. 26 May 2021. Available online: http://www.burdur.gov.tr/vali-arslantastan-senir-burdur-icme-suyu-projesine-yakin-takip (accessed on 14 April 2024).
34. Google (n.d.). Google Maps. Google Maps Metrics and Infographics. 2023. Available online: https://www.google.com/maps/place/Burdur+G%C3%B6l%C3%BC/@37.7279976,30.190126,12z/data=!3m1!4b1!4m6!3m5!1s0x14c42986f5308b8f:0x8da6bb2edc1c810!8m2!3d37.7328722!4d30.1704766!16zL20vMGZwd3Iw (accessed on 14 April 2024).
35. Turkish State Meteorological Service. *Turkey Climate Projections with New Scenario's and Climate Change (TR2015-CC)*; Turkish State Meteorological Service: Ankara, Turkey, 2015.
36. General Directorate of Water Management. *The Effect of Climate Change on Water Resources Project Report (TECCWRP)*; Ministry of Forestry and Water Management: Ankara, Türkiye, 2016. Available online: https://www.tarimorman.gov.tr/SYGM/Belgeler/iklim%20de%C4%9Fi%C5%9Fikli%C4%9Finin%20su%20kaynaklar%C4%B1na%20etkisi/Iklim_NihaiRapor.pdf (accessed on 14 April 2024). (In Turkish)
37. Dervişoğlu, A.; Yağmur, N.; Fıratlı, E.; Musaoğlu, N.; Tanık, A. Spatio-Temporal Assessment of the Shrinking Lake Burdur, Turkey. *Int. J. Environ. Geoinform.* **2022**, *9*, 169–176. [CrossRef]
38. Akçakaya, A.; Sümer, U.M.; Demircan, M.; Demir, Ö. Climate Change Projections for Turkey with New Scenarios. The General Directorate of Meteorology, Research Department, Climatology Branch Directorate. 1 July 2015. Available online: https://www.mgm.gov.tr/iklim/iklim-degisikligi.aspx?s=projeksiyonlar (accessed on 14 April 2024).
39. Abujayyab, S.K.M.; Almotairi, K.H.; Alswaitti, M.; Amr, S.S.A.; Alkarkhi, A.F.M.; Taşoğlu, E.; Hussein, A.M. Effects of Meteorological Parameters on Surface Water Loss in Burdur Lake, Turkey over 34 Years Landsat Google Earth Engine Time-Series. *Land* **2021**, *10*, 1301. [CrossRef]
40. Kılıç Germeç, H. Assessment of the Impacts of Future Climatic Variations and Anthropogenic Activities on Burdur Lake Levels. Ph.D. Thesis, Middle East Technical University, Ankara, Türkiye, 2023. Available online: https://open.metu.edu.tr/handle/11511/102492 (accessed on 14 April 2024).
41. U.S. Army Corps of Engineers. *Coastal Engineering Manual (CEM), 1110-2-1100*; U.S. Army Corps of Engineers: Washington, DC, USA, 2002. [CrossRef]
42. Genc, A.N.; Vural, N.; Balas, L. Modeling transport of microplastics in enclosed coastal waters: A case study in the Fethiye Inner Bay. *Mar. Pollut. Bull.* **2020**, *150*, 110747. [CrossRef]
43. Kazeminezhad, M.H.; Etemad-Shahidi, A.; Mousavi, S.J. Application of fuzzy inference system in the prediction of wave parameters. *Ocean. Eng.* **2005**, *32*, 1709–1725. [CrossRef]

44. Numanoğlu Genç, A.; İnan, A.; Yılmaz, N.; Balas, L. Modeling of Erosion at Göksu Coasts. *J. Coast. Res.* **2013**, *165*, 2155–2160. [CrossRef]
45. Akbas, S.O.; Kulhawy, F.H. Reliability-Based Design Approach for Differential Settlement of Footings on Cohesionless Soils. *J. Geotech. Geoenviron. Eng.* **2009**, *135*, 1779–1788. [CrossRef]
46. Kasama, K.; Whittle, A.J.; Zen, K. Effect of spatial variability on the bearing capacity of cement-treated ground. *Soils Found.* **2012**, *52*, 600–619. [CrossRef]
47. Ministry of Transport and Infrastructure Türkiye. Coastal Structures Planning and Design Technical Guideline. In *Coastal Structures Planning and Design Technical Guideline*; Ministry of Transport and Infrastructure Türkiye: Ankara, Türkiye, 2016.
48. Chung, J.S. Morison Equation in Practice and Hydrodynamic Validity. *Int. J. Offshore Polar Eng.* **2018**, *28*, 11–18. [CrossRef]
49. Det Norske Veritas DNV. DNV-ST-F101 Submarine Pipeline Systems. 2021. Available online: https://www.dnv.com/oilgas/download/dnv-st-f101-submarine-pipeline-systems/ (accessed on 14 April 2024).
50. Det Norske Veritas DNV. DNV-RP-F114 Pipe-Soil Interaction for Submarine Pipelines. 2021. Available online: https://www.dnv.com/oilgas/download/dnv-rp-f114-pipe-soil-interaction-for-submarine-pipelines/ (accessed on 14 April 2024).
51. Ministry of Interior Disaster and Emergency Management Presidency. *Turkish Earthquake Resistant Building Code*; Ministry of Interior Disaster and Emergency Management Presidency: Ankara, Türkiye, 2019.